Nuclear Engineering and Design 376 (2021) 111086, https://doi.org/10.1016/j.nucengdes.2021.111086

Total Loss of Flow Benchmark in CIRCE-HERO integral test facility

P. Lorusso[+], A. Del Nevo[#], V. Narcisi[+], F. Giannetti[+], G. Caruso[+], K. Zwijsen^ , P.A. Breijder^, T. Hamidouche*, D. Castelliti*, D. Rozzia*, M. Tarantino[#]

[+] DIAEE – Nuclear Section, "Sapienza" University of Rome, Corso Vittorio Emanuele II, 244, 00186, Rome, Italy
[#] Italian National Agency for New Technologies, Energy and Sustainable Economic Development, ENEA Brasimone R.C., Camugnano (Bo), 40033, Italy
^ NRG Arnhem, Utrechtseweg 310, P.O.Box 9034 6800 ES Arnhem, The Netherlands
* Institute for Advanced Nuclear Systems, Belgian Nuclear Research Centre (SCKCEN) Boeretang 200, 2400 Mol, Belgium

ABSTRACT

In the framework of the HORIZON2020 SESAME European project, an experimental campaign has been carried out on the large Lead-Bismuth Eutectic pool integral effect CIRCE facility at ENEA Brasimone Research Center, implementing the HERO test section. This test section is aimed at supporting the development of the ALFRED design. Within the SESAME Project, three protected loss of flow accident tests have been designed and executed, identified as SE-Test1, SE-Test2, and SE-Test3. The third test (SE-Test3) has been selected by the project participants for a benchmark activity involving system thermal-hydraulic codes and coupled system thermal-hydraulic/CFD. This activity has been divided into two phases: a blind phase, and a post-test phase.

The present paper illustrates the results achieved during the post-test phase of the CIRCE-HERO benchmark activity. Four participants simulated the experimental test. Three (ENEA, SCKCEN and UNIROMA1) used different versions of RELAP5 code, i.e. RELAP5-3D and RELAP5Mod3.3, and one (NRG) used a coupled approach based on an in-house system thermal-hydraulic code (SPECTRA) and the commercial code ANSYS CFX.

The benchmark activity hereafter presented is a relevant exercise for evaluating and comparing the predictive capabilities of system thermal-hydraulic codes, CFD codes and coupled technics, in relation to phenomena occurring during the transition between forced and natural circulation (e.g. loss of flow) in a heavy liquid metals Generation IV system.

The results of the numerical exercise showed an adequate capability of the codes to reproduce the relevant phenomena involved during the experiment. The SYS-TH codes have been more accurate than SYS-TH/CFD in predicting the trend of the main parameters during the transient, reproducing them with quite satisfactory accuracy. SYS-TH/CFD simulation, instead, provided a more satisfactory representation of the pool thermal stratification.

The results highlighted that the planning and the execution of experiments fully devoted for the code V&V process is needed for the further development of such numerical tools, in particular for SYS-TH/CFD coupled approaches, whose use is more recent respect to SYS-TH codes.

1 INTRODUCTION

Experimental programmes in scaled down integral test facilities are conducted for solving open issues of current nuclear power plant designs, for demonstrating the technical feasibility of new generation designs and for generating reference databases in order to support codes development and assessment (Annunziato et al., 1996). Experimental data are fundamental for demonstrating the reliability of computer codes in simulating the behaviour of a nuclear power plant during a postulated accident scenario: in general, this is a regulatory requirement (IAEA, 2002). International efforts have been lavished to promote and organize activities aimed at increasing confidence in the validity and accuracy of analytical tools and demonstrating the competences of the involved institutions (Umminger et al., 2012). Relevant examples of those activities are the International Standard Problems (ISPs) (OECD/NEA, 2000) under the umbrella of the Nuclear Energy Agency - Committee on the Safety of Nuclear Installations (NEA/CSNI), the Coordinated Research Projects (CRPs) sponsored by the International Atomic Energy Agency (IAEA) (IAEA, 2014a, 2014b, 2017), but also analytical exercises carried out and documented in the framework of national and European projects connected with experimental programmes in test facilities (Narcisi et al., 2019a; Uitslag-Doolaard et al., 2019).

In the framework of the HORIZON2020 SESAME (Simulations and Experiments for the Safety Assessment of MEtal cooled reactors) European project (SESAME Project, 2015), an experimental campaign has been carried out on the large LBE (Lead-Bismuth Eutectic) pool integral effect CIRCE (CIRColazione Eutettico) facility at ENEA Brasimone Research Centre (Tarantino et al., 2011), implementing the HERO (Heavy liquid mEtal pRessurized water cOoled tubes) Test Section (TS) (Rozzia et al., 2017), aiming at supporting the development of the ALFRED (Advanced Lead Fast Reactor European Demonstrator) design (Frignani et al., 2017).

Three Protected Loss Of Flow Accident (PLOFA) tests (Lorusso et al., 2019a) have been designed and executed, identified as SE-Test1, SE-Test2, and SE-Test3. These tests start with the same initial conditions, with the facility in "quasi" steady state conditions. The Fuel Rod Simulator Bundle (FRSB) power is selected in order to have about 80°C of coolant temperature difference between inlet and outlet, according to the design mass flow rate, achievable by the argon injection system. The secondary side is also operated in its nominal conditions, i.e. with the water entering at 335°C and the steam outlet pressure set at 17.2 MPa. During PLOFA transients, FRSB power is decreased following a decay heat curve equal for the three tests. Furthermore, in SE-Test1, argon

injection is set to 0 kg/s and feedwater to 30% of nominal mass flow rate in 2 s (simulation of Decay Heat Removal system – DHR). SE-Test2 differs from the first one only for the feedwater reduction to 0% in about 2 s. SE-Test3 simulated the DHR mode with a feedwater reduction to 30% in 2 s and the reactor pump flywheel by a argon reduction based on a defined table.

The third test, SE-Test3, has been selected by the project participants for a benchmark activity involving SYStem Thermal-Hydraulic (SYS-TH) codes, and coupled SYS-TH/CFD. This activity is divided into two phases: i) a blind phase, where the participants have simulated the transient on the basis of boundary and initial conditions available by the test design plus characterization data provided by the experimental team; and ii) a post-test phase following the distribution of the experimental data of the test. The present article illustrates the post-test phase of the benchmark.

The relevance of the test SE-Test3 is related to the prototypical geometry of the test section, the heavy liquid metal (LBE) used as coolant in the primary system and the availability of an instrumentation system adequate, through the analysis of the experimental data, to characterize the transient conditions and to support the assessment of predictive numerical tools. The measurement system allows the characterization of the temperature distribution in the FRSB, in the HERO TS primary system and in the pool for standalone or coupled code assessment. In agreement with the benchmark purposes, focus is given to the loss of flow integral test and in the onset of the natural circulation in case of small distance between the heat source and heat sink thermal barycenters. The analysis is accompanied by a heat transfer assessment in the FRSB and the double wall tubes prototypical steam generator.

The post-test calculations are carried out by four Institutions: ENEA, SCKCEN, and Sapienza University of Rome (UNIROMA1), using standalone SYS-TH codes, i.e. RELAP5-3D and RELAP5/Mod3.3* (implementing properties of LBE. Pb, PbLi), and NRG using a coupling approach between SPECTRA and ANSYS CFX.

2 PLANNING OF THE ANALYTICAL EXERCISE

2.1 CIRCE-HERO experimental set-up

CIRCE is a pool-type experimental facility designed and realized at ENEA Brasimone R.C., in Italy (Lorusso et al., 2018a). The facility consists of a primary system using LBE as coolant and a secondary system cooled by demineralized water. The primary system is mainly composed of (Pesetti et al., 2017): a cylindrical vertical main vessel 8.5 m high, filled with about 70 tons of molten LBE, with argon as cover gas, a storage tank, a transfer tank, LBE heating and cooling systems and auxiliary systems for LBE circulation and the gas recirculation. The main vessel hosted several test sections designed time by time on the basis of the features of the experiments, inserted inside from the top of the vessel and fixed on the upper part through a coupling flange.

The new TS (see *Figure 1*), named HERO, has been obtained from the previous one named ICE (Integral Circulation Experiment) (Tarantino et al., 2015), replacing the heat exchanger designed for the previous experimental campaigns with a new one: a Steam Generator Bayonet Tube (SGBT) type, composed of 7 bayonet tubes with geometry and operating conditions relevant for lead fast reactors (see blue component in *Figure 1*). The SGBT unit is partially contained in the shell of the previous heat exchanger (see *Figure 1*). All the other components are the same of the pre-existing TS: the FRSB for the LBE heating, composed of an electrical bundle with 37 pins (in red in *Figure 1*) arranged in a wrapped hexagonal lattice with a pitch to diameter ratio (p/d) equal to 1.8 and an active length of 1 m, the fitting volume (in green), the riser (in yellow) and the separator (in gold) on the top. Only the separator has been modified to adapt its geometry with the new SGBT features (higher lateral walls and improved bottom plate).

During the normal operation, LBE is heated inside the FRSB and it is driven through the fitting volume and the riser up to the separator, acting as hot pool, where the hot LBE is collected. Then, primary coolant enters the SGBT unit from dedicated inlet holes and it flows along the shell side, returning cooled to the pool and closing in such a way the path. A dedicated argon injection device is located at the inlet section of the riser for performing enhanced circulation of the primary coolant (gas lift). The injected gas flows up along the riser and it is separated from the LBE in the separator.

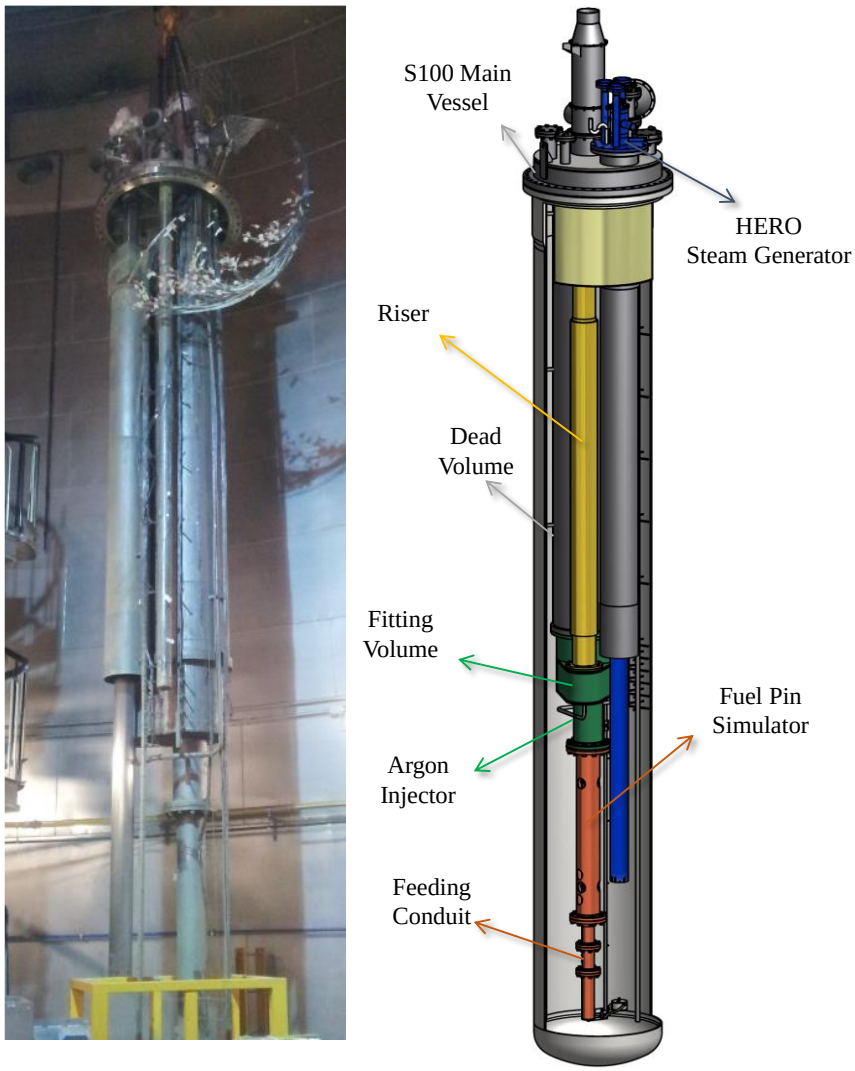

Figure 1 ***CIRCE-HERO Primary Loop (main vessel and HERO Test Section)***

The HERO SGBT unit is a scaled mock-up (1:1 in length) of the ALFRED steam generator. It consists of a tube bundle of 7 bayonet tubes arranged in a hexagonal shell with a triangular pitch and a p/d of 1.42. Each tube has an active length of about 6 m and it is composed of four coaxial tubes, as represented in *Figure 2*: the water flows downwards through the Slave Tube reaching the bottom part of the bayonet tube. Then, it rises passing through the annular region between the First Tube and Second Tube, where the steam is produced. The gap between Slave Tube and First Tube is filled with air acting as insulator, avoiding the steam condensation in the annular region. The gap between the Second Tube and Third tube is filled with AISI316L Stainless Steel powder slightly pressurized by helium at about 8 bar. The pressurization of the gap allows easier detections of any leakages, increasing the plant safety. A dedicated helium line has been realized for pressurizing the stainless steel powder gap of bayonet tubes at ~8 bar. Concerning the conductivity of the gap filled with steel powder + He, several studies have been performed at ENEA Brasimone R.C. on this topic. Specific experimental campaigns have been executed on dedicated experimental facilities (Rozzia et al., 2015a) for the investigation on the powder thermal performances. The analysis highlighted that the steel powder thermal conductivity is a function of the temperature and it is influenced by different factors, i.e. the grain size and growth, powder compaction, thermal cycling. Experimental sensitivity analysis on such parameters has been performed and experimental correlations have been derived (Rozzia et al., 2015b). Since the activity reported in Rozzia et al., 2015b has been the basis for the selection of material for the construction of the HERO steam generator, the correlations reported in Rozzia et al., 2015b have been taken as reference for the simulations.

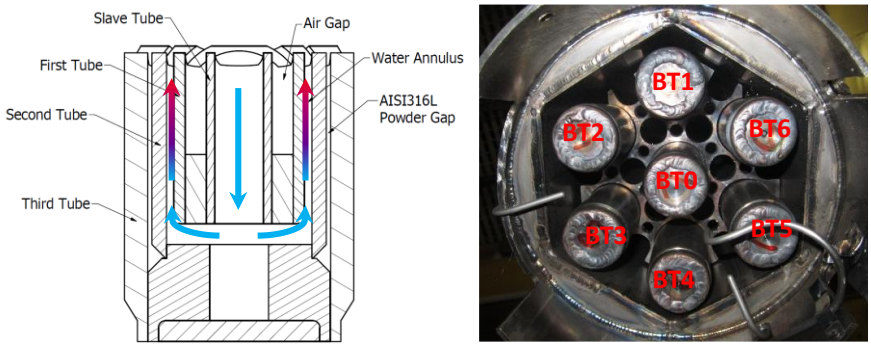

Figure 2 – Sketch of the bayonet tube geometry (left) and bottom view of the tube bundle (right)

The instrumentation installed in the primary system is composed of an overall number of about 170 thermocouples (TCs), 10 bubble tubes, one Venturi flow meter and three LBE level meters. Two pressure transmitters are set in the main vessel cover gas. Moreover, an argon flow meter measures the normal litres per second injected in the riser, for gas lift occurrence. A total of 119 TCs are positioned in the pool to gather information on mixing and stratification feedback, maintained in the same position of ICE TS (Tarantino et al., 2015). Three TCs have been added and positioned accordingly with the expected thermal stratification level, predicted with a pre-test analysis realized by the RELAP5-3D© SYS-TH code (Narcisi et al., 2018), obtained improving the pre-existing numerical model of the ICE TS (Narcisi et al., 2017).

Each component of the TS is thermally characterized by means of thermocouples located at the inlet and outlet sections (e.g. fitting volume, riser, separator). In particular, the FRSB and the SGBT shell side are instrumented by bulk TCs and wall TCs, positioned at the inlet/outlet sections and at different elevations for a better monitoring of the temperatures along of their active lengths (Lorusso et al., 2019b). *Figure 3* and *Figure 4* show the TCs installed along the FRSB and the shell side of the HERO SGBT, respectively.

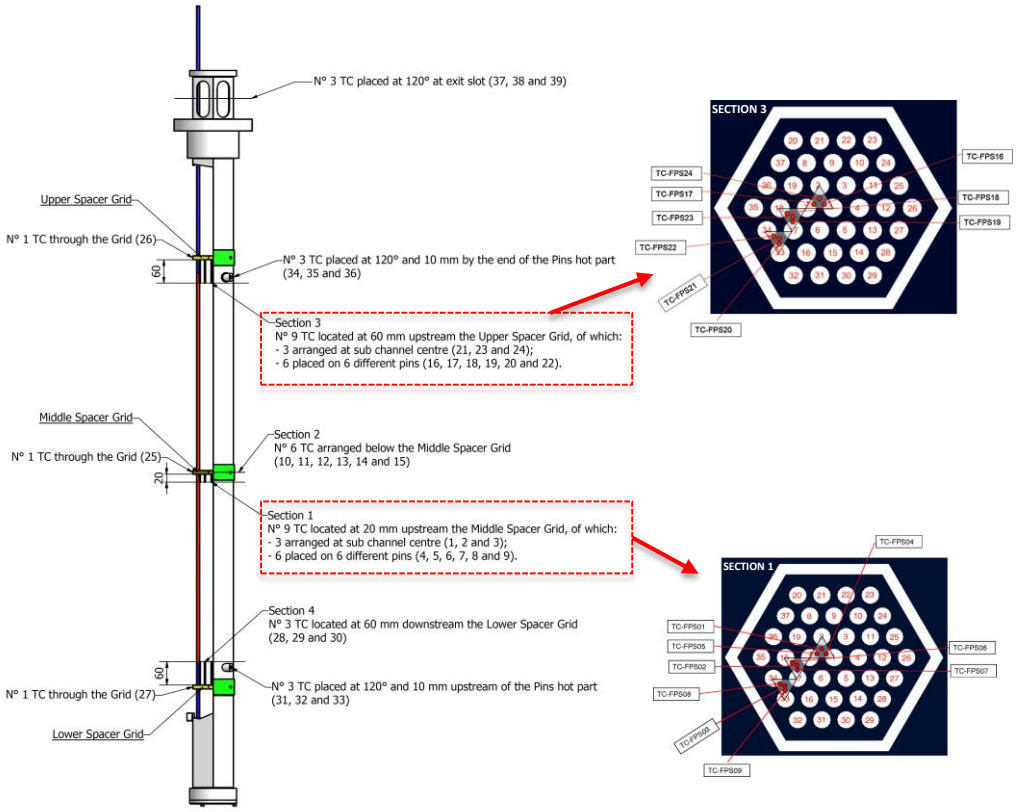

Figure 3 – Instrumentation installed along the FRSB

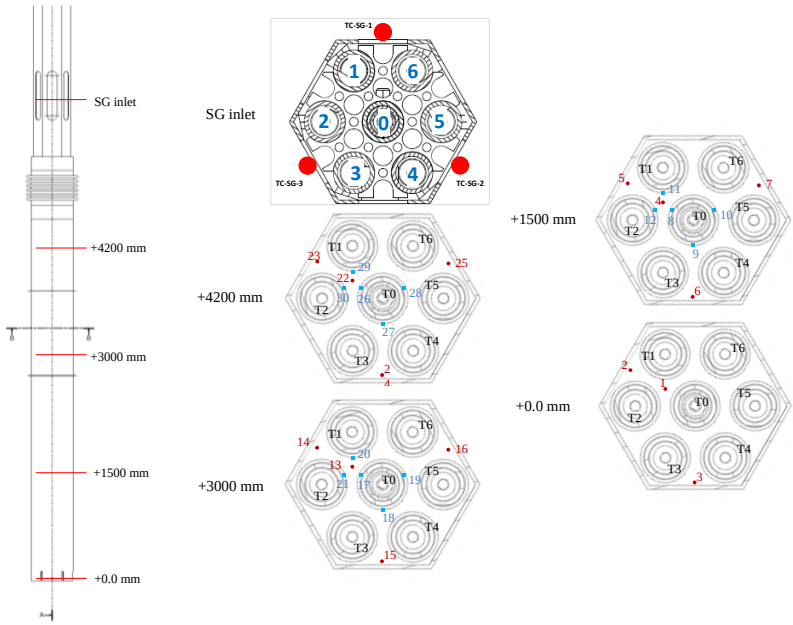

Figure 4 – Instrumentation installed on the LBE Side of the HERO SGBT: red dots are the bulk TCs, light blue dots are the wall TCs

A secondary once-through loop (Figure 5) has been realized to feed the HERO SGBT with demineralized water (Lorusso et al., 2018b). It mainly consists of: a demineraliser, a volumetric pump, a helical pre-heating system, a manifold with seven outlet ½" tubes connected to the inlet of the Double Wall Bayonet Tubes (DWBTs) and a 3" line to discharge the steam produced in the HERO SGBT to the environment. The pressure along the loop is maintained at the operating value through a dedicated regulation valve located downstream the SGBT. A ¾" bypass line has been realized for the start-up phases, equipped with its own regulation valve.

The secondary loop instrumentation is composed of 32 TCs, 9 relative and 4 differential pressure transmitters, one Coriolis flow meter and 7 mini Turbine Flow Meters (TFMs), installed upstream each DWBT. Water temperature and pressure are monitored at the heater, manifold and DWBTs inlet and outlet sections, as well as downstream the regulation valves. Differential pressure measurements across 4 DWBTs will characterize single and two-phase pressure losses. Three thermocouples set at the steam chamber exit aim to detect possible condensation and radial stratification. Concerning the tube bundle, 7 TCs are positioned at the inlet section of each DWBT (TC-TX-I), while 4 TCs measure the water temperature at the outlet section of the tubes T0, T1, T3, T4 (TC-CX-O70). The central tube (named as T0), is equipped with 5 TCs set in the rising annulus of the DWBT at different levels (+500 mm, +1500 mm, +3000 mm, +4200 mm, +6000 mm, assuming as 0 mm the DWBT bottom) aiming at characterizing water vaporization. Details of the secondary loop and SGBT instrumentation are reported in Figure 5.

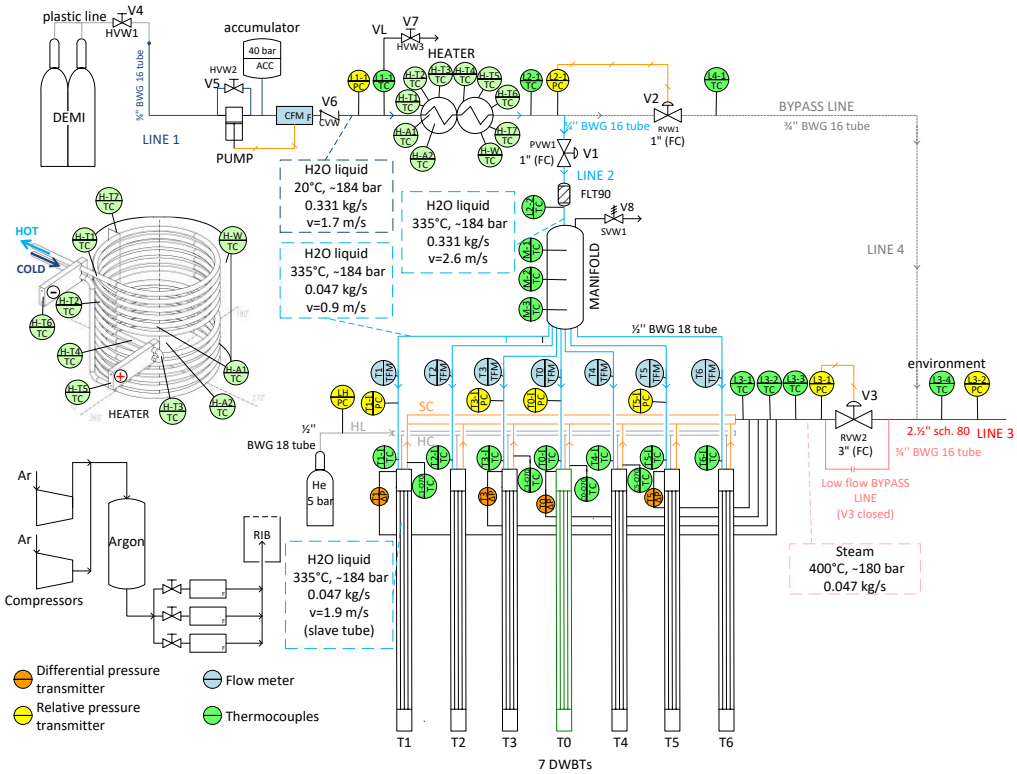

Figure 5 – Secondary loop P&ID (Lorusso et al., 2018b)

2.2 CIRCE-HERO SESAME Test SE-TEST3

The tests realized consist of PLOFA scenarios, occurred during the normal operation of the facility. The nominal working conditions, for both primary and secondary loops, have been maintained constant for a time lapse relevant for the analysis of the phenomena involved; after that, the transition has been carried out, managing the FRSB power supplied, the argon injection device and the water mass flow rate to the HERO Steam Generator (SG). After the transient, the system continues to operate with the primary loop working in Natural Circulation (NC) regime and the HERO SG acting as decay heat removal system. In particular, the transient test SE-TEST3 (Lorusso et al., 2019a) has been assumed as reference test for the benchmark calculations.

The experimental boundary conditions assumed before and after the transient are summarized in *Table 1* (from Lorusso et al., 2019a). In nominal working conditions, the power supplied by the FRSB is about 356 kW (*Figure 6*), to compensate the power removed by the HERO SGBT and the heat losses to the environment; the LBE mass flow rate is maintained in forced circulation regime with an argon flow rate of 2.75 Nl/s. In the secondary loop, the water temperature at the inlet section of the DWBTs is maintained at about 336°C. The water mass flow rate is measured by the mini-turbine flow meters installed upstream the inlet section of each bayonet tube, achieving a total of ~0.26 kg/s, assuming a water density of ~640 kg/m^3 and a uniform distribution of the water flow among the 7 tubes. This assumption results to be a simplification, since the measures of the TFMs are affected to the uncertainty of the instrumentation and a small spread among the values has been observed (*Figure 7*). Alternatively, the water mass flow rate can be calculated applying the thermal balance equation on the heater component, obtaining a value of ~0.29 kg/s.

During the transient, the FRSB power is reduced according to a characteristic heat decay curve, while the loss of the primary pump is simulated by the reduction of the argon flow rate injection from 2.75 Nl/s to 0 with a curve reproducing the pump flywheel (*Figure 6*).The water mass flow rate is reduced to 30% (~0.08 kg/s) in a time ramp of 2 s, as shown in *Figure 7*. The loss of signals of TFM-T3 and TFM-T5 in SE-TEST3 is due to the low flow rate achieved after the transient, which is close to the lower limit of the measure range of the instruments. The beginning of the transients for the FRSB power, argon flow rate and water mass flow rate occur simultaneously.

Figure 8 (left) reports the LBE mass flow rate achieved during the test. Before the transient, in gas-enhanced circulation regime, the value achieved is about 34 kg/s, which decreases rapidly when the gas injection is disabled. After the transient, the mass flow rate reaches the value of about 6 kg/s when the natural circulation is established. The experimental trend demonstrates that, despite the small distance difference between the heating source (FRSB) and the heat sink (SGBT), the LBE natural circulation establishes successfully, assuring a satisfactory cooling of the heating source, under decay heat conditions. The same figure (right) also reports the LBE temperature trends at the FRSB inlet and outlet. At the outlet section the temperature decreases significantly due to the power decrease, passing from 496 °C to the minimum value (446 °C) immediately after the transient, and then reaching a maximum of 465 °C, from which it starts to decrease slowly, when NC of the LBE is established. The temperature at the FRSB inlet section remains at ~420 °C, with a low decrease after the transient.

Before the transient, the LBE temperature at the SGBT inlet section (*Figure 9*, left), is about 480 °C, while after the cooling it is ~408 °C. After the transient, both the inlet and outlet LBE temperatures start to decrease smoothly, without abrupt changes. From such temperature data, considering the LBE mass flow rate reported in *Figure 8* (left) and calculating a LBE heat capacity from the

recommended correlation proposed in (OECD/NEA, 2015), it is possible to calculated the power removed from the HERO LBE side equal to about 385 kW. Such values takes into account the power removed by the secondary side and the eventual fraction of heat exchanged toward the pool.

The pool thermal stratification is reported in *Figure 9* (right). Before the transient, the maximum temperature reached is ~475 °C, in the upper part of the pool, while the lower value is ~420 °C in the lower part. After the transient, the temperature profile is shifted to lower values, with a maximum/minimum temperature reached of 468 °C/406 °C. The thermal stratification in the LBE pool occurs in vertical direction only, with uniformity along the horizontal planes.

Finally, *Figure 10* reports the water conditions is terms of temperature (left) and pressure (right). At the DWBTs inlet section, the temperature is maintained constant at ~336 °C for the entire test, excepting for oscillations during the flow rate transient. Such flow rate reduction leads to a steam temperature sudden increase from an average value of ~360 °C to ~450 °C. Then, the temperature decreases due to the lower thermal field in the primary system (SG shell side), with the consequently reduction of power removed.

Table 1 – SE-TEST3, experimental boundary conditions at the start and the end of the transient

Parameter	Unit	Start of Transient (t=0s)	End of Transient (t=1800s)
FRSB Power	[kW]	356	20
Argon flow rate	[Nl/s]	2.75	0
Water	[kg/s]	0.29	0.08
Water SG T_{inlet}	[°C]	~336	~336

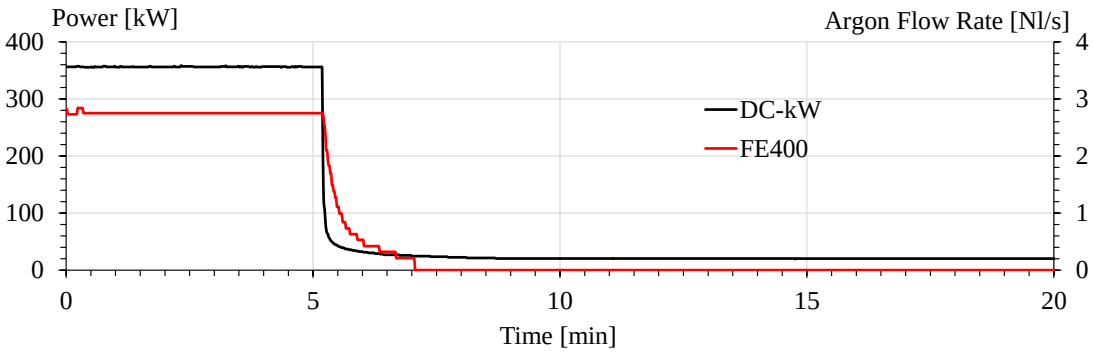

Figure 6 – SE-TEST3, FRSB Power and argon Flow Rate experimental trends (from Lorusso et al., (2019a))

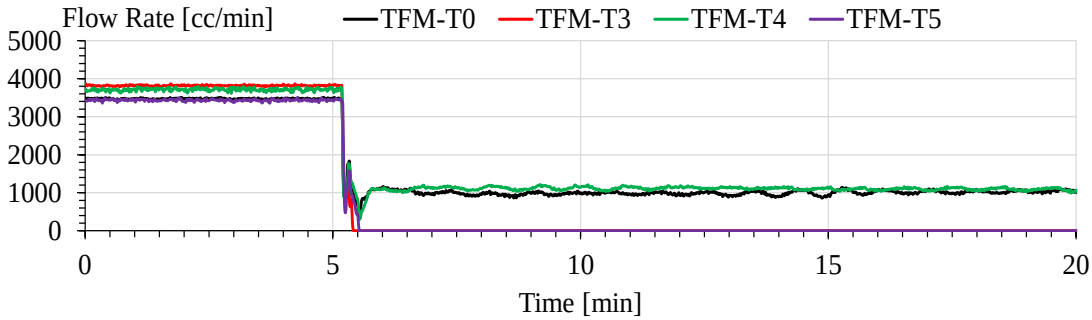

Figure 7 – SE-TEST3, H2O mass flow rate trends during the PLOFA Test measured by turbine flow meters (from Lorusso et al., (2019a))

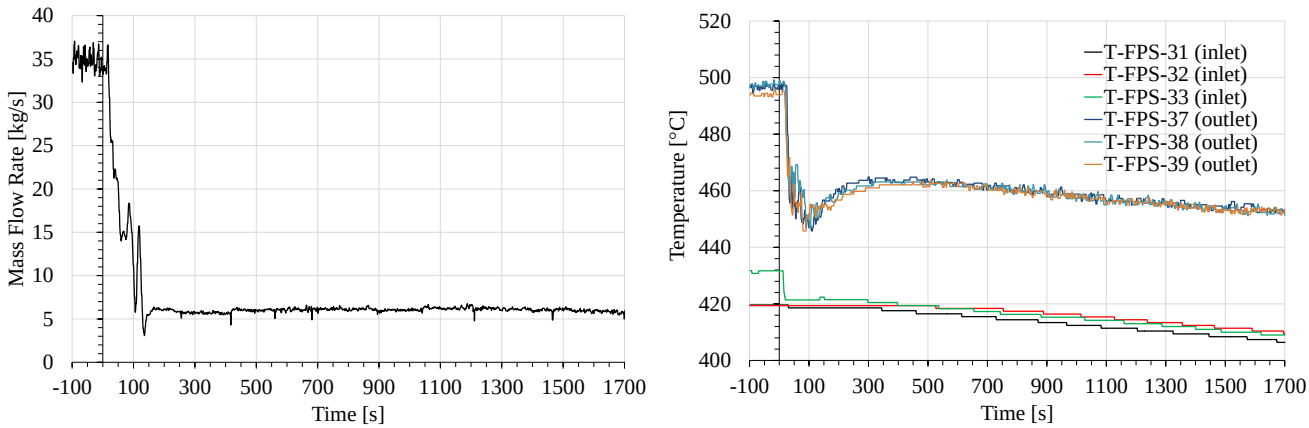

Figure 8 – SE-TEST3, LBE mass flow rate (left) and LBE temperature at the FPS inlet and outlet sections (right)

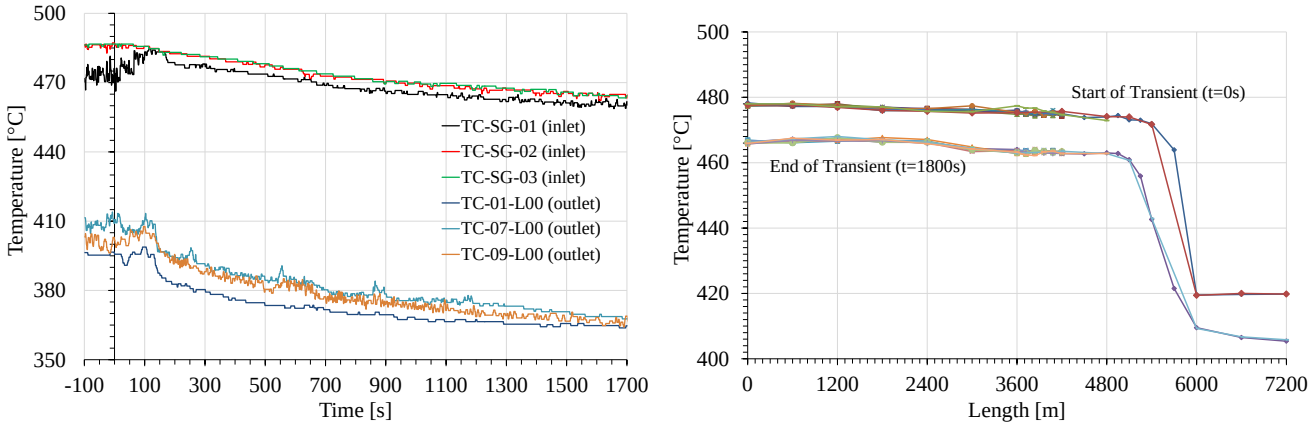

Figure 9 – SE-TEST3, LBE temperature at the SGBT inlet and outlet sections (left) and pool thermal stratification (right)

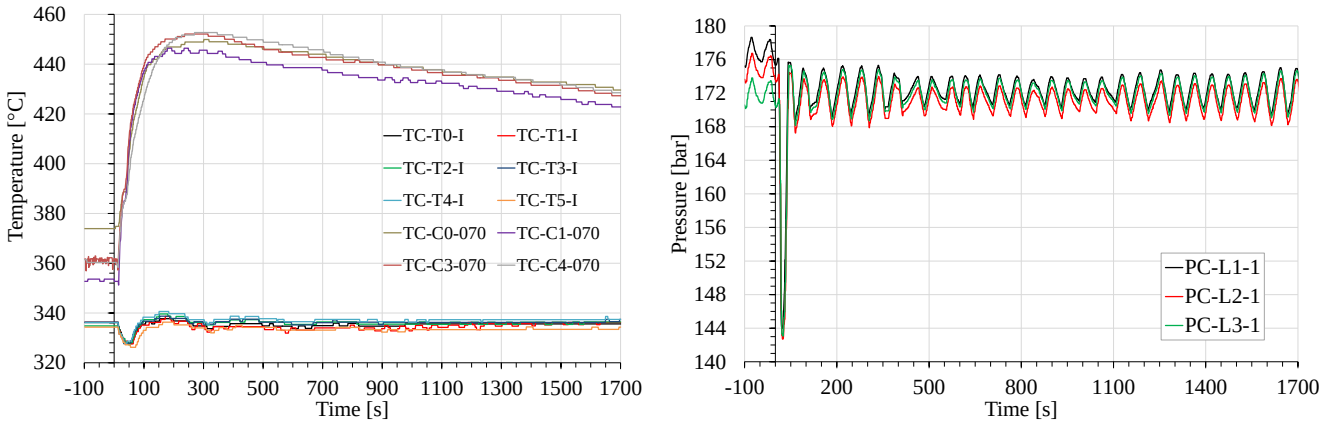

Figure 10 – SE-TEST3, H2O temperature at the SGBT inlet and outlet sections (left) and water pressure (right)

3 MODELS DEVELOPED BY PARTICIPANTS

The post-test calculations have been performed by four Institutions with the following codes:

- ENEA used standalone SYS-TH code RELAP5/Mod3.3 (RELAP5/Mod3.3 code manual, 2003), customized implementing properties of LBE. Pb, PbLi (NEA-Handbook, 2007) and three relevant heat transfer correlations for HLMs (Oriolo et al., 2000; Tarantino et al., 2012; Martelli et al., 2019);
- Sapienza University of Rome (UNIROMA1) used standalone SYS-TH code RELAP5-3D v4.3.4 (RELAP5-3D© Code Manual, 2015), including as default the appropriate heat transfer package for liquid metal cooled systems. In the version used by UNIROMA1, the LBE thermodynamic properties correlations were revised in the research activity described in Balestra et al., (2016), integrating the most recent correlations recommended in OECD/NEA, (2015);
- SCKCEN used standalone SYS-TH code RELAP5-3D v4.0.3, including as default the modifications and additions implemented by INL (Davis and Shieh, 2000) concerning the appropriate heat transfer package for liquid metal cooled systems and the thermal-physical properties of LBE. Such RELAP5-3D standard properties, have a deviation within +/-5% to +/-7% for volumetric heat capacity and thermal conductivity (Hamidouche, 2013) respect to the ones recommended by OECD expert group (OECD/NEA, 2015);
- NRG used a coupling approach between the SYS-TH code SPECTRA (Stempniewicz, 2017) and ANSYS CFX.

3.1 Description of the nodalizations

3.1.1 ENEA – RELAP5/Mod3.3

ENEA RELAP5 nodalization of the CIRCE-HERO facility (see *Figure 11*) has been set-up by up-grading the former CIRCE-ICE nodalization (Tarantino et al., 2012), thus it keeps the same basic modelling approach. It can be divided into three main parts: the pool zone, the main circulation zone (including the FRSB, the riser and the LBE side of HERO test section), and the secondary system, i.e. the water side of the HERO test section. The elevations of the different parts of the facility are maintained in the nodalization. A sliced approach is applied at all zones, LBE and water systems. The node to node ratio is kept uniform with a maximum ratio of 1.2 between adjacent sub-volumes. The heat transfer correlations applied in the LBE zone are Ushakov in the bundle and Seban-Shimazaki, elsewhere. The energy loss coefficients in the junctions are evaluated or estimated on the basis of the system geometry. The material proprieties are taken from reference documentation (Pesetti et al., 2018a).

Feeding pipe – FRSB. The feeding conduit is modelled with pipe components including the FRSB active part. Thermal structures are modelled according to the description of the facility in Pesetti et al., (2018a). They allow a thermal connection between the inner pipe rising part and the pool zone.

Rising leg (Fitting volume – riser – separator). The bottom part of the riser is connected to the gas injection line in which the imposed mass flow rate of argon is injected. Downstream the riser, the separator is modelled with two branch elements. Analogously with the lower part, thermal structures connect thermally the riser and separator with the pool zone. The upper part is connected with the cover gas of the pool, whereas the bottom part is connected with the HERO test section. Multiple junctions connect the two stacks of hydraulic volumes.

HERO SGBT primary side. The HERO primary side is modelled with two pipes representing the central part and the peripheral part of the LBE channel, respectively: one pipe component represents 85% of the flow area and it is thermally coupled with the secondary side, whereas the other is thermally connected with the dead zone of the pool surrounding the HERO test section. The LBE SG outlet is represented by a junction connecting the last volume of the SG component with the pool zone.

Main Pool. The pool zone is modelled with three stacks of hydraulic volumes, having the same axial discretization. At each axial elevation, there is a connection modelled with a multiple junction component. This subdivision is not adopted on the top and bottom zones. Indeed, the upper part is modelled with five branch components. The LBE free level is in the CV-111. The heat losses of the pool are modelled connecting the LBE hydraulic volumes with imposed boundary conditions, through the vessel structures (metal and insulation). The nodalization of the pool is connected on the top with a time dependent volume which imposes the pressure conditions of the cover gas. Heat losses are modelled at the pool outer boundary, using environmental temperature and Heat Transfer Coefficient (HTC)=2.85 W/(m^{2}K), and at the in-pool dead volume where the air gas is forced to keep the temperature of the electrical connections at acceptable values (i.e. about 100°C).

Secondary side. The secondary system is modelled with two time dependent volumes and one time dependent junction components for setting the boundary conditions; two pipes and representing the steam generator tubes (descending part and annular ascending part) and one branch modelling in dummy way the steam manifold downstream the SG tubes. Thermal structures model the heat exchange between the inner tube and the outer tube of the DWBT, as well as the LBE/water heat exchange.

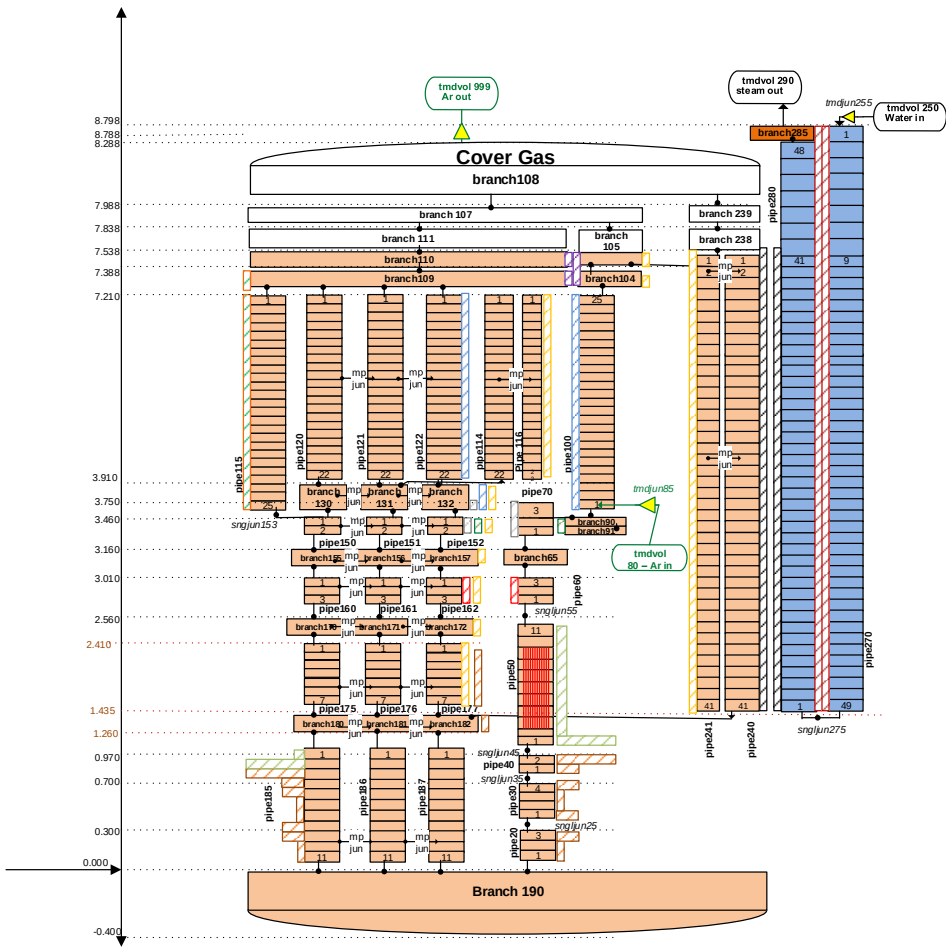

Figure 11 – ENEA, RELAP5/Mod3.3*: CIRCE-HERO nodalization sketch.

3.1.2 University of Rome Sapienza – RELAP5-3D v4.3.4

The nodalization scheme of CIRCE-HERO, adopted for the pre-test simulations (Narcisi et al., 2018; Lorusso et al., 2019c), has been developed starting from the thermal-hydraulic model of CIRCE-ICE, validated with experimental data (Narcisi et al., 2018). The pressure losses of the main flow path were calibrated in CIRCE-ICE post-test analysis (Narcisi et al., 2019b), except for the new SG. Local pressure drop coefficients, depending on the flow conditions, have been introduced for the Venturi flow meter and the grids installed through the FRSB and the SG. For the calculation of grid's pressure losses, the Rehme correlation with the correction factor proposed in Schikorr et al., (2010) has been implemented in the model.

For the HTC evaluation, Seban-Shimazaki is adopted for non-bundle geometries. In bundle geometry, the Westinghouse correlation was obtained in the p/d range between 1.1 and 1.4; it means that the ratio of both FRSB and SG are out of the validity range. As highlighted in Giannetti et al., (2016), the Ushakov correlation (Ushakov et al., 1977) provides a better estimation of the HTC than Westinghouse correlation, maintaining a similar trend of Nu versus Pe. For these reasons, two constant multiplicative factors have been applied to the HTC evaluation on the LBE side of FRSB (1.31) and SG (1.02) LBE side, to correct the heat transfer coefficient according to the Ushakov correlation.

The geometrical scheme consists of two macro-regions (*Figure 12*): a mono-dimensional model, reproducing the primary flow path and the secondary system, and a multi-dimensional model, simulating the pool of the facility.

Feeding pipe – FRSB. The feeding conduit is modelled as a pipe component. Heat transfer between this component and the pool is neglected, since large temperature differences are not expected in these two zones. The FRSB is simulated with a sub-channel modelling approach, consisting of 72 mono-dimensional parallel pipes. The mass transfer between the adjacent channels is reproduced with cross junctions, evaluating the hydraulic resistance with a form loss coefficient dependent of the flow conditions (Idelchik, 1986). The FRSB is simulated by means of heat transfer active nodes (active length) and heat transfer passive nodes, taking into account the rods thermal inertia in the upper part of the FRSB and inside the fitting volume, as well as the heat dissipation through the FRSB hexagonal wrap (including the stagnant LBE within the region between the hexagonal wrap and the cylindrical shell which contains the FRSB unit). The radial conduction between adjacent channels is reproduced by means of additional passive heat transfer nodes, assuming a "fake" material with the LBE thermal conductivity and a negligible heat capacity. A more detailed description of the sub-channel modelling approach is presented in Narcisi et al. (2019b, 2019c).

Rising leg (Fitting volume – riser – separator). Two vertical pipes connect the FRSB channels to the fitting volume and the fitting volume to the separator, respectively. A time dependent junction simulates the Ar mass flow rate injection, while the Ar inlet conditions are set with a time dependent volume. Above the separator, the gas-plenum of the facility is modelled with a vertical pipe connected, below with the separator and the pool, and above with a time dependent volume that imposes the pressure of the gas.

HERO SGBT primary side. The SG primary side is simulated with an equivalent pipe component, composed of 43 control volumes.

Main Pool. The multi-dimensional component developed for the pool simulation (Narcisi et al., 2019c) consists of 51 axial levels, 4 radial meshes and 8 azimuthal sections. The axial discretization has been developed to match thermocouples positions inside the pool and to respect the sliced modelling approach. The volume occupied by the internal components are taken into account with porosity factors, evaluated on the basis of the actual geometries of the facility. The heat losses between the primary flow path and the pool and towards the external environment are fully integrated in the model. The environment is simulated as boundary conditions, setting the environment temperature to 20°C and imposing a constant value of the heat transfer coefficient on the external surface of the insulated vessel.

Secondary side. A detailed nodalization of the secondary system has been developed, including the feeding pipe downstream the pre-heater, the manifold, seven DWBTs separately simulated, the steam chamber and the steam line up to the outlet regulation valve. The components which simulate the secondary system are considered adiabatic toward the environment. Each DWBT model includes two vertical pipes, reproducing the feed-water descending side and the annular riser (simulated with an annular component) and two heat structure components, simulating the heat exchange between the descending and the ascending side of the bayonet element and the power transferred between primary and secondary systems. Two time dependent volumes impose the feedwater inlet temperature downstream the pre-heater and the secondary system pressure at the outlet of the test section, respectively, while a time dependent junction sets the total water mass flow rate upstream the feeding line. A K-loss coefficient is imposed at the inlet of each DWBT, to reproduce the presence of the turbine flow meter. In Narcisi et al. (2019c) the measurements on the secondary side were fully investigated. The analysis of the experimental acquisitions highlighted an uncertainty of the secondary flow rate distribution through the DWBTs. For this reason, the K-loss coefficients at the inlet of the tubes have been calibrated in order to obtain the correct outlet temperature during the full power operation.

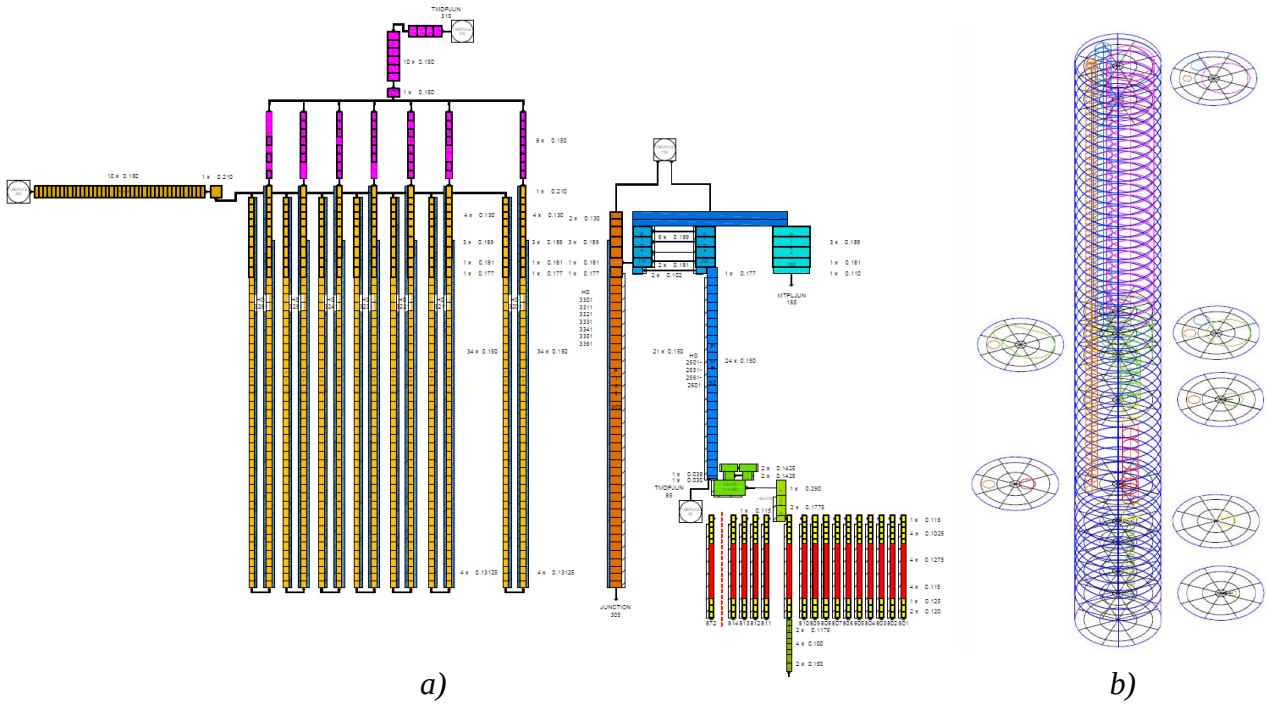

a) *b)*

Figure 12 – UNIROMA1, RELAP5-3D: mono-dimensional model (a) and multi-dimensional model (b).

3.1.3 SCKCEN – RELAP5-3D v4.0.3

The CIRCE-HERO 1D nodalization is depicted in *Figure 13*. The data used for the development of the nodalization are taken from Rozzia et al., 2016 and Pesetti et al., 2018a. The stagnant fluids (LBE around the FRSB and air around the riser and the HERO) are modelled as structures and the corresponding thermos-physical properties are derived from tabulated data for LBE (NEA-Handbook, 2007) and air (Ashare handbook, 2009). The thermal-physical properties for the powder conductivity assumed are the ones provided in the benchmark specifications (Pesetti et al., 2018a).

In general, a sliced approach is used for the cell dimensions (height or length), with some exception, in order to match the thermocouples positions in the CIRCE-HERO facility.

For heat transfer in the FRSB, the Westinghouse correlation (Kazimi and Carelli, 1976) has been used, assuming a p/d=1.1 and a tuned fouling factor in order to match the Ushakov correlation (Ushakov et al., 1977) in the full range of CIRCE operation conditions. The same procedure is considered for HERO to use the Ushakov correlation, whereas the Seban-Shimazaki correlation is adopted for all other internals and vessel representative structures.

Feeding pipe – FRSB. The FRSB is represented by one single channel and its associated heat structure representing the 37 electrically heated rods. The pressure loss coefficient through the Venturi flow meter has been calibrated at nominal power and mass flow rate conditions using the experimental data provided after the experiment (Lorusso et al., 2019a), whereas the bundle grids and spacer pressure losses coefficients were evaluated using the correlations discussed in Mikityuk (2009) and Idelchik (1986).

Rising leg (Fitting volume – riser – separator). The argon injection at the inlet of the riser is modelled using a time dependent volume and a time dependent junction. The argon mass flow rate is tuned in order to reach the nominal flow rate of the experiment. On top of the separator, the cover gas pressure is controlled by a time dependent volume representing a boundary condition for the system.

HERO SGBT primary side. The primary side of the HERO is modelled by a pipe subdivided in appropriate axial sub volumes in order to track the temperature of LBE and tube wall matching the positions of the thermocouples.

Main Pool. The pool is also modeled using one pipe with adapted section as function of the elevation. This choice is motivated by the objective of investigating the limitations of the use of 1D volumes in the steady state and the transient from forced to natural circulation. Heat losses through the vessel wall were calibrated versus the dedicated heat losses experimental data (Pesetti et al., 2018b).

Secondary side. The secondary cooling system is modelled starting from the inlet of the manifold up to the end of the steam line (upstream valve outlet regulation valve) (Pesetti et al., 2018a). As boundary conditions for the secondary system, the exit pressure is fixed according to the experimental data, whereas the inlet water temperature and mass flow rate are imposed at the manifold inlet.

The seven DWBTs are modelled individually considering the design specification provided in Pesetti et al., (2018a). Heat structures are introduced to simulate heat exchange between the descending and the ascending side of the BTs and the power transferred between primary and secondary systems. The localized pressure losses in the pool are obtained from Mikityuk (2009).

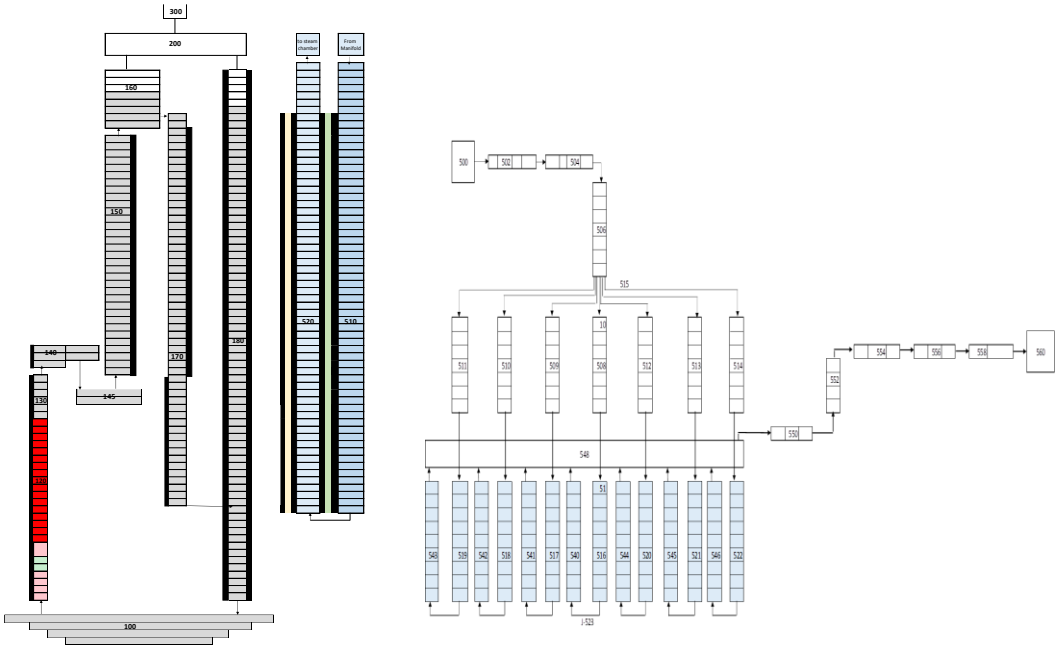

a) *b)*

Figure 13 – SCKCEN, RELAP5-3D: nodalization of the primary cooling system (a) and secondary cooling system (b).

3.1.4 NRG – SPECTRA SYS-TH / ANSYS CFX CFD coupled code

NRG created a multi-scale model of the CIRCE-HERO facility to perform the benchmark test, coupling a CFD code with a SYS-TH code. The SYS-TH model of the CIRCE-HERO facility is set-up by the SPECTRA SYS-TH code (Stempniewicz, 2017). The nodalization of the SYS-TH model is shown in *Figure 15*, for which data from Pesetti et al. (2018a) are used and it consists of the FRSB, the feeding conduit, the fitting volume, the riser, the separator, the complete HERO SGTB together with secondary side (where the seven tubes are combined), and the LBE pool including all the heat structures representing the walls of the structures.

The CFD code ANSYS CFX is used to model the main pool and vessel of the CIRCE-HERO facility. The CAD used in the CFD simulations is shown in the right of *Figure 14*. The internal elements indicated by the arrows are removed from the CAD, so that only the region between the external vessel wall and the structure walls remains, i.e., the main pool. The CFD geometry only extends up till the free surface to avoid multi-phase flow calculations.

The coupling approach used for the CFX-SPECTRA coupled calculations is based on a domain-overlapping two-way approach and is schematically depicted in *Figure 15*. Temperature of the LBE is exchanged between the two codes on the inlet and outlet of the CFD domain, i.e., SPECTRA provides CFX with a temperature at the outlet of HERO (inlet of CFX), while CFX in return couples the temperature of LBE at the FRSB inlet (CFX outlet) back to SPECTRA. SPECTRA also provides the LBE mass flow rate at HERO's outlet to CFX. As the inner loop has only one inlet and outlet, this mass flow rate is also used at the FRSB inlet as boundary condition for the CFD code.

The non-wall resolved mesh used for the CFD calculations, which is depicted in the left of *Figure 14* for the area around the separator, consists of in total 1.8M cells. Most of these cells are hexahedral shaped, though difficult regions with corners, such as in the bottom of the vessel, contain tetrahedral cells. The velocity field is solved using the RANS SST k-ω turbulence model with automatic wall functions, while the thermal energy model is used to produce the temperature field. As the liquid in question is a heavy metal, a turbulent Prandtl number of 2.0 is used (Bricteux et al., 2012).

Feeding pipe – FRSB. The main heat source in the CIRCE facility, the FRSB, is modelled with 10 axial heat structure nodes, with an additional node at each end representing mixing zones. Furthermore, the feeding conduit and the release pipe of the facility are included in the model as four axial nodes before the FRSB and three axial nodes after the FRSB, respectively.

Rising leg (Fitting volume – riser – separator). The fitting volume is located above the release pipe and is discretized into four nodes, allowing both horizontal and vertical flow. The riser is modelled with 12 axial nodes, while the separator consists of the top four nodes.

HERO SGBT primary side. The HERO SGBT is modelled with 26 axial nodes and comprises of three segments, of which one is the LBE primary side.

Main Pool. The LBE pool has the same axial nodalization as the inner structures, except at the bottom, where only one control volume is used around the feeding conduit. The control volumes comprising the pool are horizontally connected with the inner loop structures through heat structure walls to allow heat transfer between the inner loop and main pool. The thickness and properties of the heat structures are according to data given in Pesetti et al. (2018a). Portions of walls consisting of more than one material, e.g., the

riser, which has a layer of air between two concentric metallic cylinders, contain more heat structures than those consisting of a single material, like the fitting volume whose wall is made of AISI 304 only.

Secondary side. The secondary side of the HERO SGBT consists of two concentric rings in which water flows downwards and subsequently upwards. Feedwater mass flow rate, temperature and pressure are prescribed at the inlet of the secondary side of HERO. Heat structures are also included to allow heat transfer between the three tubes. The model consists of seven separate tubes lumped together as one SG.

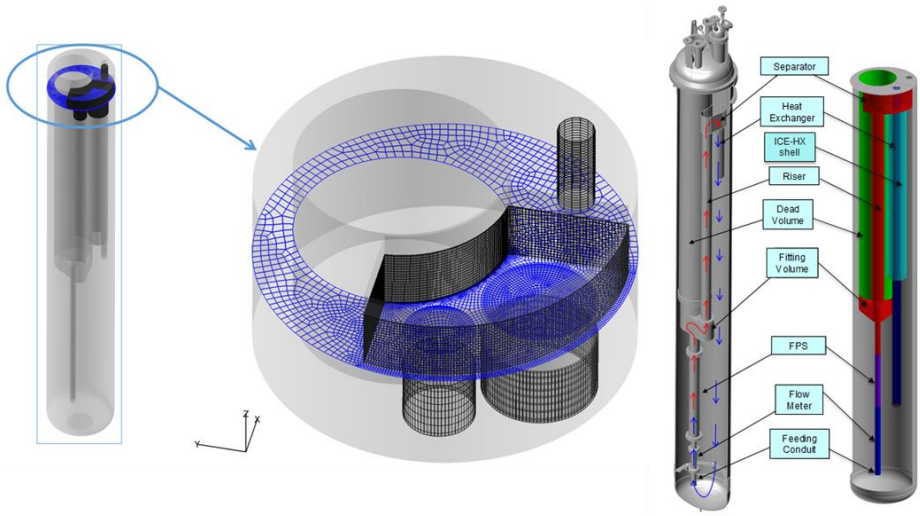

Figure 14 – NRG, SPECTRA/CFX: CIRCE-HERO CFD computational model.

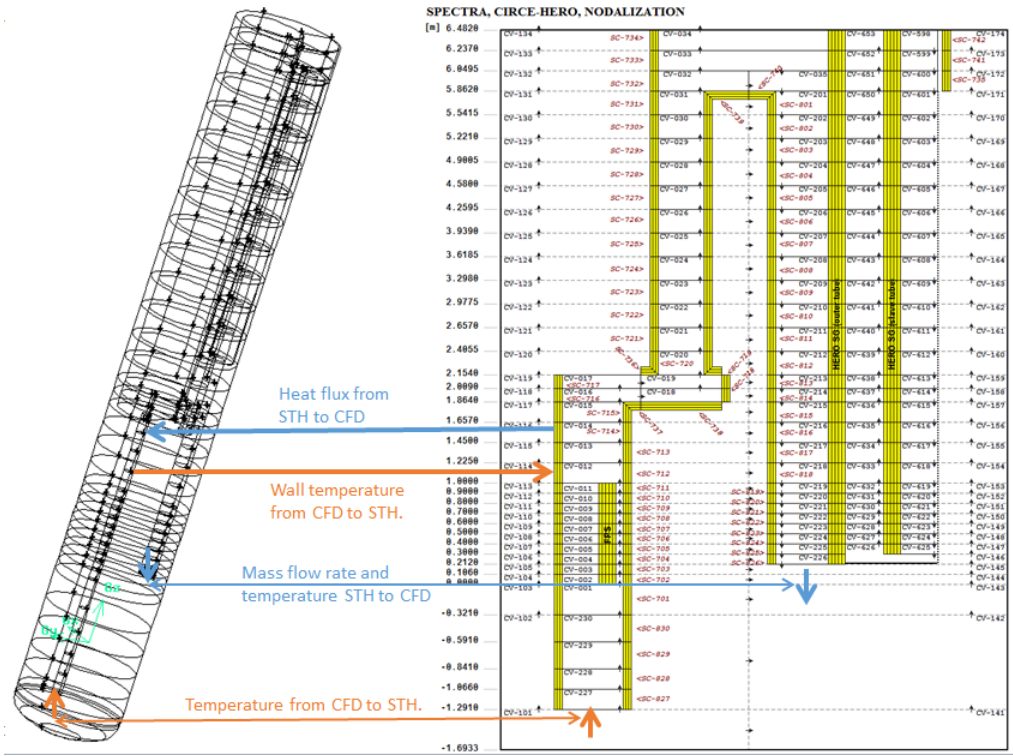

Figure 15 – NRG, SPECTRA/CFX: CIRCE-HERO computational domain for CFX-SPECTRA coupled calculations.

3.2 Comparison of participants nodalizations

The information provided by the participants about the adopted TH-SYS and CFD codes and nodalizations are compared in *Table 2*, *Table 3* and *Table 4*. In particular, *Table 3* provides information about the adopted code resources, the nodalization features and the main code options. *Table 4* reports the geometrical characteristics of the nodalizations, focusing on the modeling of the facility in terms of hydraulic volumes and thermal structures. Finally, the main elevations of the models are reported in *Figure 16*. The analysis of the data brings the considerations as follows (Del Nevo et al., 2019).

- Different modelling approaches are tested.

- ENEA and SCKCEN use 1D components and feature the pool zone with 3 parallel pipes (ENEA) and 1 pipe (SCKCEN) respectively.
- UNIROMA1 exploits the capabilities of the MULTID component of RELAP5-3D, used for the modelling of the pool, and of a sub-channel modelling approach, used for the FRSB. This results in a complex nodalization with almost 3k hydraulic volumes.
- NRG assesses a more advanced simulation approach based on the coupling between the 1D modelling of the facility, by means of the in-house system code SPECTRA and the 3D representation, featured with ANSYS CFX for the simulation of the LBE pool.
- Different approaches have been used by participants for modelling the 7 DWBTs. ENEA and NRG adopted the averaging method by representing the tube bundle with one average pipe. UNROMA1 and SCKCEN model the tubes one by one.

- Comparable number of axial nodes are used for the modelling of the FRSB, but SCKCEN and UNIROMA1 with 16 hydraulic volumes have a more detailed tracking of the coolant and structures temperatures.
- Different heat transfer correlations are applied for the bundle zones: UNIROMA1 and SCKCEN corrected the default RELAP5-3D correlation with a multiplication factor compensating the difference with Ushakov at steady state conditions, ENEA applied Ushakov. NRG used a user-defined variant of the Mikityuk-correlation.
- Considering the coolant volumes in the circulation loop (from feeding conduit entrance up to HERO outlet) the SYS-TH nodalizations highlight differences in the zone between the FRSB outlet and fitting volume inlet (UNIROMA1) and in the separator zone (SCKCEN). It should be noted that in case of separator zone the difference can be explained also with the modelling of the separator.
- SYS-TH and CFD hydraulic modellings of the pool are comparable, with the exception of SCKCEN nodalization which shows a difference in the zone between the Top of Active Fuel (TAF) and the fitting volume. NRG CFD mesh does not represent the upper part of the facility, above the free volume.
- The heat losses from the pool toward the environment have been set up on the bases of heat losses characterization tests Pesetti et al., (2018b), which have been provided to the participants for calibrate their models.
- Differences are observed in the volumes of the heat structures, i.e. in the FRSB and in the other passive structures.
- There is a general good agreement between the elevations in the nodalizations of participants.

Table 2 – Summary of the codes used and the modelling approaches adopted by the participants

Participant	Code used	Modeling approach
ENEA	RELAP5/Mod3.3	1D components
UNIROMA1	RELAP5-3D v4.3.4	1D components/ MULTID components /sub-channel approach for FRSB
SCKCEN	RELAP5-3D v4.0.3	1D components
NRG	SPECTRA SYS-TH / ANSYS CFX CFD coupled code	1D (SPECTRA) / 3D (ANSYS CFX)

Table 3 – CIRCE-HERO SE-Test3 benchmark, general information: nodalizations and code options.

#	QUANTITY	**ENEA** R5-M3.3	**SCKCEN** R5-3D	**UNIROMA1** R5-3D	**NRG** SPECTRA/CFX
1	**ADOPTED CODE RESOURCES**				
1-1	Total number of hydraulic nodes primary system	412	205	2844	65 (loop) 68 (pool)
1-2	Total number of hydraulic nodes secondary side (HERO)	52	1121	755	56
1-3	Total number of mesh points in the FRSB heat structures	70	27	17568	60 (for each pins)
1-4	Total number of mesh points in the DWBT heat structures	2251	432	15400	156 / 261 / 252[(1)]
1-5	Total number of mesh points in the heat structures	3908	3590	37953	888
2	**NODALIZATION FEATURES / MODELLING CHOICES**				
2-1	Hydraulic model (3-D or 1-D component) – FRBS region	1-D	1-D	1-D	1-D
2-2	N. of hydraulic channels in FRBS region (ring and angular sectors for 3D components)	1	1	72	10
2-3	Total number of axial nodes - FRBS region	11	16	16	10
2-4	Crossflow junctions between parallel channels in FRBS region	NO	NO	YES	NO
2-5	Hydraulic model (3-D or 1-D component) –SG primary system	1-D	1-D	1-D	1-D
2-6	N. of hydr. channels in SG primary system (ring and angular sectors for 3D components)	2	1	1	26
2-7	Total number of axial nodes - SG primary system	41[(2)]	53	40	26
2-8	Crossflow junctions between parallel channels in SG primary system	YES	NO	NO	NO

2-9	N. of hydr. meshes modelling SG secondary system DWBTs	97	102 x7	95 x7	56
2-10	Hydraulic model (3-D or 1-D component) – POOL region	1-D	1-D	3-D	3-D
2-11	N. of hydr. channels in POOL region (ring and angular sectors for 3D components)	3	1	4 - 8	CFD
2-12	Total number of axial nodes - POOL region	55	70	50	CFD
2-13	Crossflow junctions between parallel channels in POOL region	YES	NO	YES	YES
2-14	Modelling of POOL-environment heat losses	YES	YES	YES	YES
2-15	Modelling of riser-POOL heat transfer	YES	YES	YES	YES
2-16	Modelling of SG-dead zone heat transfer	YES	YES	YES	NO
3	**CODE OPTIONS**				
3-1	Heat transfer correlation in FRBS region (LBE-structure) (3)	Ushakov	Westinghouse (4)	Westinghouse (4)	Mikityuk
3-2	Heat transfer correlation in SG primary system (3) (LBE-structure)	Ushakov(5)	Westinghouse (4)	Westinghouse (4)	Mikityuk
3-3	Heat transfer correlation in non-bundle geometry	Seban-Shimazaki	Seban-Shimazaki	Seban-Shimazaki	Seban-Shimazaki
3-4	Pressure drop correlation in FRBS region	Colebrook-White	Rehme	Colebrook-White	--
3-5	Pressure drop correlation in SG primary system	Colebrook-White	default	Colebrook-White	--

(1) *156 for HERO LBE side/Pool, 261 for LBE/2nd side and 252 for 2nd water/2nd steam.*
(2) *Considering the pipe where the primary to secondary heat exchange occurs.*
(3) *Details of the correlations used for bundle geometries reported in Table 5*
(4) *tuned by means of a fouling factor in order to match the Ushakov correlation*
(5) *fouling factor 0.9*

Table 4 – CIRCE-HERO SE-Test3 benchmark, nodalizations development: geometrical information (part 1 of 2)

#	QUANTITY	UNIT	ENEA R5-M3.3	SCKCEN R5-3D	UNIROMA1 R5-3D	NRG SPECTRA/CFX
1	**PRIMARY CIRCUIT HYDRAULIC VOLUMES**					
1-1	Feeding conduit – up to BAF	m^3	0.0091	0.0099	0.0073	NA
1-2	FRBS active – from BAF to TAF	m^3	0.0060	0.0060	0.0060	NA
1-3	Upper FRBS zone including fitting volume and riser – from TAF to separator	m^3	0.4003	0.4094	0.3094	NA
1-4	Separator – up to vessel top flange	m^3	0.2070	0.1196	0.2272	NA
1-5	HERO SG mock-up primary system	m^3	0.0469	0.0453	0.0456	NA
1-6	Total integral circulation volume	m^3	0.6694	0.5902	0.5956	NA
1-7	Pool zone 1 – from bottom to BAF	m^3	1.8199	1.3113	1.7023	1.706(1)
1-8	Pool zone 2 – from BAF to TAF	m^3	1.0115	1.0399	1.0495	1.049 (1)
1-9	Pool zone 3 – from TAF to fitting volume	m^3	1.0566	0.5607	1.0492	0.903(1)
1-10	Pool zone 4 – from fitting volume to separator	m^3	2.8295	2.5777	2.4506	2.465(1)
1-11	Pool zone 5 – from separator to vessel top flange	m^3	0.5169	1.1592	0.6524	--(2)
1-12	Total pool volume	m^3	7.2344	6.6489	6.9041	6.478 (1)
2	**SECONDARY CIRCUIT HYDRAULIC VOLUMES**					
2-1	Manifold	m^3	--	2.746E-04	2.160E-04	--
2-2	DWBT central descending tubes - 7 tubes (total)	m^3	2.035E-03	2.039E-03	2.012E-03	--
2-3	DWBT annular rising tubes - 7 tubes (total)	m^3	3.370E-03	3.412E-03	3.331E-03	--
2-4	Secondary side steam collector and tube up to valve V3 (steam regulation valve)	m^3	3.750E-03(3)	3.184E-02	1.195E-02	--
3	**HEAT TRANSFER SURFACE AREAS**					
3-1	FRBS (total) – ACTIVE	m^2	0.953	0.636	0.953	--
3-2	HERO – inner tube, outer surface	m^2	3.009	1.358	3.050	--
3-3	HERO – outer tube, outer surface	m^2	4.483(4)	2.100	4.395	--
3-4	HERO casing – outer surface	m^2	3.603	1.411	3.011	2.987(5)
3-5	FRBS casing – from BAF to fitting volume – outer surface	m^2	1.155	0.680	1.175	0.599
3-6	Fitting volume – outer surface	m^2	1.589	0.181	2.455	1.163(6)
3-7	Riser – outer surface	m^2	3.004	1.266	2.503	2.563

3-8	Separator – outer surface	m^2	1.107	0.413	3.631	0.950
3-9	Pool – inner surface	m^2	30.302	15.423	22.285	29.573
4	**HEAT STRUCTURES VOLUMES**					
4-1	FRBS	m^3	1.954E-03	7.575E-02	1.954E-03	--
4-2	Feeding conduit entrance up to fitting volume bottom w/o FRBS	m^3	4.570E-02	4.422E-02	5.004E-02	--
4-3	Fitting volume	m^3	1.331E-02	8.139E-03	3.156E-02	--
4-4	Riser	m^3	0.078	0.019	0.055	--
4-5	Separator	m^3	0.009	0.004	0.012	--
4-6	Pool vessel steel	m^3	0.460	0.481	0.469	--
4-7	HERO casing	m^3	0.058	0.024	0.056	--
4-8	DWBT slave plus first tube	m^3	7.766E-03	1.604E-03	6.219E-03	--
4-9	DWBT air gap between the slave – first tubes	m^3	6.210E-03	8.068E-04	6.293E-03	--
4-10	DWBT second plus third tube	m^3	2.021E-02	2.995E-03	1.851E-02	--
4-11	DWBT gap between second – third tubes	m^3	2.165E-03	2.898E-04	1.983E-03	--

(1) *Value related the CFX nodalization.*
(2) *Not modelled with CFX.*
(3) *Dummy value. The component is not modelled in its full geometry.*
(4) *Active part is 3.488 m^2.*
(5) *The value includes 0.047 m^2 at bottom where no tubes are.*
(6) *The value includes top and bottom*

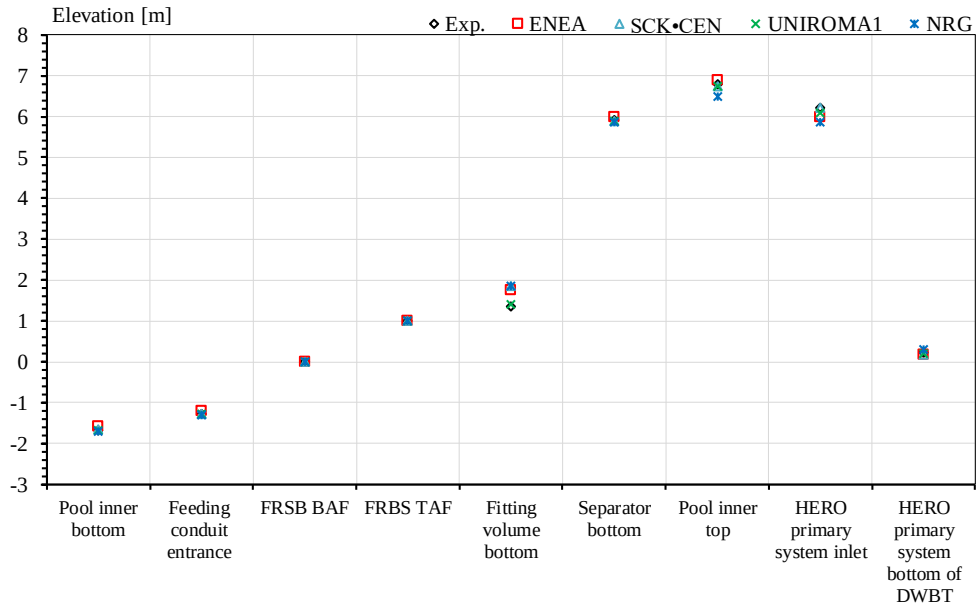

Figure 16 – CIRCE-HERO SE-Test3 benchmark, nodalizations development: comparisons among relevant elevations.

Table 5 – Correlations used for convective heat transfer of HLMs in bundle and non-bundle geometries

Correlation	Equation	Range of validity
Seban-Shimazaki	$Nu = 5.0 + 0.025Pe^{0.8}$	Non bundle geometry
Ushakov	$Nu = 7.55\frac{p}{d} - 20\left(\frac{p}{d}\right)^{-13} + \frac{3.67}{90\left(\frac{p}{d}\right)^2} Pe^{\left(0.56+0.19\frac{p}{d}\right)}$	Bundle geometry $1.3 < p/d < 2.0$ $1 < Pe < 4000$
Mikityuk	$Nu = 0.047\left(1 - e^{-3.8\left(\frac{p}{d}-1\right)}\right)(Pe^{0.77} + 250)$	Bundle geometry $1.1 < p/d < 1.95$ $30 < Pe < 5000$
Westinghouse	$Nu = 4.0 + 0.33\left(\frac{p}{d}\right)^{3.8}\left(\frac{Pe}{100}\right)^{0.86} + 0.16\left(\frac{p}{d}\right)^5$	Bundle geometry $1.1 < p/d < 1.4$ $10 < Pe < 5000$

Nu – Nusselt number
p/d – pitch over diameter ratio
Pe – Peclet number

4 CIRCE-HERO NUMERICAL BENCHMARK

The objective of the benchmark activity is to evaluate and to compare the predictive capabilities of SYS-TH, CFD codes and coupled technics in relation to phenomena occurring during the transition between forced and natural circulation (e.g. loss of flow) in HLM Generation IV system (Forgione et al., 2018). This implies the:

- understanding of phenomena/processes recorded in the transient;
- assessing and comparing the predictive capabilities of codes in the domains of interest;
- identifying limitation of the existing best estimate codes and coupling approach;
- developing a common understanding and promoting an exchange of experience and knowledge;
- drawing a support on the possible use of the codes for regulatory framework and the industry.

The relevant phenomena/processes expected during the transient are:

- Transition from forced (gas-enhanced) to natural circulation;
- Heat transfer in the FRSB;
- Heat transfer primary to secondary side;
- Conduction in fluid and structures;
- Multidimensional coolant temperatures in core;
- Heat transfer in passive structures and heat losses (e.g. riser, HERO external shroud, vessel);
- Stratification in pool;
- Pressure drop.

4.1 Comparison and evaluation of steady state results

The evaluation of the steady state requires the comparisons between experimental measures and the calculated results at the beginning of the transient. Additionally, quantities are requested to evaluate the set-up of boundary conditions (see *Table 6*). Table 7 reports the following quantities: the experimental measurements, the codes results including the errors referred to the selected data of the test. In the tables, the ID of the measurements are also included for sake of completeness.

Table *8* reports the uncertainties related to the performed measurements, calculated combining the standard deviations with the TCs uncertainties.

The considerations summarized hereafter are based on the results provided by the participants.

- FRSB power is correctly set-up by the participants. Nevertheless, as the power balance is concerned, differences are observed. The power exchanged in HERO test section calculated by UNIROMA1 differs from the other participants, being 62 kW larger than the FRSB power supplied. Concerning the heat losses calculated between the pool and the environment, the participants set their model according to the outcomes of the characterization reported in (Pesetti et al., 2018b), predicting values of heat losses close to the 34 kW at 400°C, achieved during the experimental characterization tests. Finally, the heat exchange calculated between the feeding conduit, the riser and the pool highlights a scatter from the lower values (i.e. 3 kW) and the highest, i.e. 18.7 kW, predicted by the ENEA simulation.
- The LBE coolant temperatures at FRSB inlet and outlet are well reproduced by the participants, with the exception of SCKCEN, which evidenced over-prediction of the FRSB inlet temperature equal to 5.3°C. The differences between the temperature increase across the FRSB calculated by the participants, let it suppose that the thermo-physical properties implemented in the code are comparable. Considering the temperatures at HERO inlet, it is observed that the coolant temperature experiences a temperature decrease of about 11°C from the FRSB outlet and the HERO inlet, due to the heat losses from the fitting volume, riser, and separator toward the pool. This trend is well simulated by NRG and UNIROMA1 and underestimated by ENEA. HERO coolant outlet temperature is largely over-estimated by the participants (i.e. 21.2°C SCKCEN, 14.0°C ENEA, 11.5°C UNIROMA1), with the exception of NRG, showing a value comparable with the experimental datum.
- The steam temperature outlet recorded in the SG secondary side is well simulated by the participants, with the exception of NRG, which overestimates the experimental value of 45°C. It should be noted the participants set the feedwater mass flow rate with values ranging from 0.29 kg/s (NRG) to 0.34 kg/s (UNIROMA1).
- The primary system mass flow rate at the Start of Transient (SoT) is well simulated by ENEA and SCKCEN. Larger errors are observed in UNIROMA1 and NRG simulations.
- The pressure drop vs. length plot is reported in Figure 17. Discrepancies are observed mainly in the feeding conduit and FRSB pressure drops evaluation by the participants.

Table 6 – CIRCE-HERO SE-Test3 benchmark, nodalizations development: steady state boundary conditions.

#	Quantity	ID	Unit	Exp.	**ENEA** R5-M3.3 Y_{calc} (ε) [3]	**SCKCEN** R5-3D Y_{calc} (ε) [3]	**UNIROMA1** R5-3D Y_{calc} (ε) [3]	**NRG** SPECTRA/CFX Y_{calc} (ε) [3]
1	**POWER BALANCE**							

1-1	Core thermal power	DC-kW	kW	356	356.0 *(0.0%)*	356.0 *(0.0%)*	356.0 *(0.0%)*	356.0 *(0.0%)*
2	**ABSOLUTE PRESSURES**							
2-2	Secondary system steam line pressure	PC-L3-1	MPa(g)	17.1	17.2 *(0.6%)*	17.08 *(-0.1%)*	17.1 *(0.6%)*	17.0 *(-0.6%)*
3	**COOLANT TEMPERATURES**							
3-5	Secondary side DWBT SG inlet (manifold zone)	TC-M2	°C	336.7	336.0 *(-0.7°C)*	335.0 *(-1.7°C)*	336.5 *(-0.2°C)*	336.9 *(0.2°C)*
4	**FLOW RATES**							
4-1	Ar injection	FE400	nl/s	2.75	2.72 *(-1.1%)*	NA	2.75 *(0.0%)*	--[1]
4-3	Feedwater total	0.26/0.29[2]	kg/s	--	0.308 *(--)*	0.330 *(--)*	0.340 *(--)*	0.294 *(--)*

(1) *Not available (the recirculation flow was imposed in the junction entering the riser)*
(2) *TFMs/Thermal balance equation on the heater component*
(3) *Calculated value and absolute or relative error with respect to the experimental datum*

Table 7 – CIRCE-HERO SE-Test3 benchmark, nodalizations development: steady state results.

#	Quantity	ID	Unit	Exp.	ENEA R5-M3.3 Y_{calc} (ε) [5]	SCKCEN R5-3D Y_{calc} (ε) [5]	UNIROMA1 R5-3D Y_{calc} (ε) [5]	NRG SPECTRA/CFX Y_{calc} (ε) [5]
1	**POWER BALANCE**							
1-2	HERO power exchanged	--	kW	--	351.6 *(--)*	353.3 *(--)*	418.0 *(--)*	358.0 *(--)*
1-3	Pool vessel heat losses	--	kW	--	37.3 *(--)*	33.8 *(--)*	30.2 *(--)*	37.9 *(--)*
1-4	Feeding conduit and riser – pool heat exchange	--	kW	--	18.7 *(--)*	2.97 *(--)*	3.0 *(--)*	7.97 *(--)*
2	**ABSOLUTE PRESSURES**							
2-1	Pool cover gas	PE007	MPa(g)	0.014	0.02 *(42.9%)*	0.014 *(0.0%)*	0.0075 *(-46.4%)*	NA
3	**COOLANT TEMPERATURES**							
3-1	LBE FRSB inlet [4]	T-FRSB-31 T-FRSB-32 T-FRSB-33	°C	419.6 419.4 431.7[3]	419.6 *(0.1°C)*	424.8 *(5.3°C)*	420.5 420.5 *(1.0°C)* 420.5	419.7 *(0.2°C)*
3-2	LBE FRSB outlet [4]	T-FRSB-37 T-FRSB-38 T-FRSB-39	°C	495.5 497.8 495.2	493.2*(-3.0°C)*	496.8 *(0.6°C)*	495.6 495.6 *(-0.5°C)* 495.6	493.8 *(-2.3°C)*
3-3	LBE HERO inlet [4]	TC-SG-01 TC-SG-02 TC-SG-03	°C	470.3[3] 485.3 485.3	489.4 *(4.1°C)*	495.8 *(10.5°C)*	488.3 *(3.0°C)*	483.7[1] *(-1.6°C)*
3-4	LBE HERO outlet [4]	TC-01-L00 TC-07-L00 TC-09-L00	°C	395.7 413.4 400.9	417.4*(14.0°C)*	424.5 *(21.2°C)*	414.8 *(11.5°C)*	400.7 *(-2.6°C)*
3-6	Secondary side DWBT SG outlet (steam line zone) [4]	TC-L3-1 TC-L3-2 TC-L3-3	°C	356.7 357.8 354.7	365.3 *(8.9°C)*	352.6 *(-3.8°C)*	353.4 *(-3.0°C)*	401.4 *(45.0°C)*
3-7	Steam void fraction	--	--	--	0.99	1.0	0.8	1.0
4	**MASS FLOW RATES**							
4-2	Primary system (Venturi)	Mm(LBE)	kg/s	33.3	33.6 *(0.9%)*	33.7 *(1.2%)*	31.7 *(-4.8%)*	36.5[2] *(9.6%)*

(1) *487.7 in CV-035; 483.7 in CV-201*
(2) *28.6 in JN-204; 36.5 in JN-228*
(3) *Experimental value not considered in the evaluation of the error*
(4) *Avg. value considered.*
(5) *Calculated value and absolute or relative error with respect to the experimental datum*

Table 8 – FPS and SG temperature measurements and related uncertainties

ID	T [°C] (Avg)	Exp. Uncertainty [°C]
T-FRSB-31	419.6	±1.50
T-FRSB-32	419.4	±1.58
T-FRSB-33	431.7	±1.57
T-FRSB-37	495.5	±1.86
T-FRSB-38	497.8	±1.80
T-FRSB-39	495.2	±1.71
TC-SG-01	470.3	±3.87
TC-SG-02	485.3	±1.83
TC-SG-03	485.3	±1.72
TC-01-L00	395.7	±1.64
TC-07-L00	413.4	±2.88
TC-09-L00	400.9	±2.89

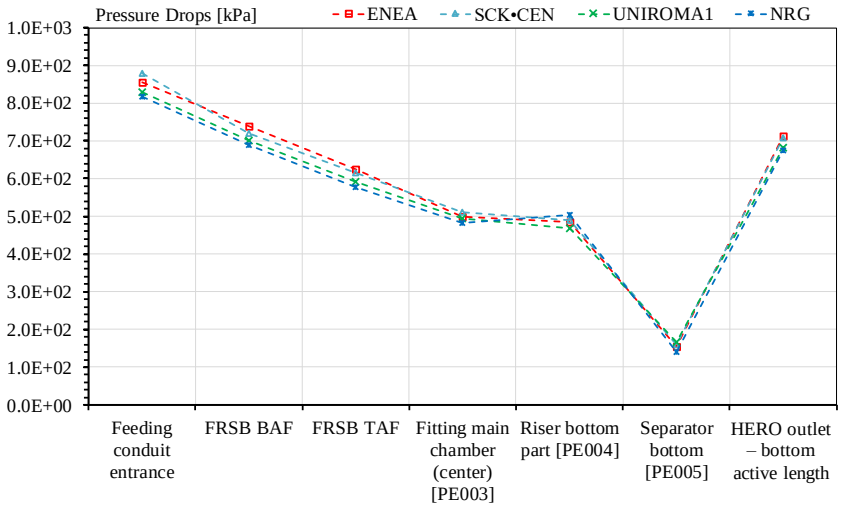

Figure 17 – CIRCE-HERO SE-Test3 benchmark, nodalizations development: primary system pressure drop vs. length.

4.2 Comparison and qualitative evaluation of reference results

The comparisons between the experimental data and the calculated results are carried out with the objective of verifying if the code simulations are capable to reproduce the experimental time trends. *Table 9* reports the list of the relevant events and the timing of their occurrences. These timings are compared with the corresponding values observed in the experiment.

The following comments apply:

- The participants predicted with an excellent accuracy the timing and quantities of the main events related to the cladding temperature minimum and maximum values.
- On the opposite the maximum value of coolant temperature at the core outlet is anticipated in all code simulations.

The time trends provided by the participants are reported hereafter, as well as the main comments about the visual observation of the selected time trends is provided, grouping the parameters into sets of homogeneous quantities. Quantitative accuracy evaluation has not been carried out. For sake of completeness, *Figure 18* provides the information related to the CPU time for executing the simulations, highlighting the increase of computational time needed to run a more detailed model.

Table 9 – CIRCE-HERO SE-Test3 benchmark: resulting sequence of main events.

#	EVENT DESCRIPTION	Unit	EXP	ENEA R5-M3.3	SCK•CEN R5-3D	UNIROMA1 R5-3D	NRG SPECTRA/CFX	Note
1	Gas enhanced circulation reduction begins (simulation of coast-down) – (LOFA)	[s]	1	1	1.	1	20	Imposed
2	SCRAM	[s]	0	0	0.	0	12	Imposed
3	Feedwater pumps reduction start	[s]	0	0	0.	1	10	Imposed
4	Feedwater pumps reduction @ 30% of nominal flow rate	[s]	3	3	2.	4	10.1	Imposed
6	Gas enhanced circulation reduction ends	[s]	113	113	113	113	150	Imposed
7	Coolant T @ FRSB outlet is minimum	[s]	79 (448°C)	80 (437.2°C)	81 (436.8°C)	81 (438.1°C)	81 (438.1°C)	
8	Maximum Cladding T reaches the minimum (value in °C)	[s]	79 (435°C)	81 (439°C)	82 (437.2°C)	81 (436°C)	81 (434°C)	
9	Maximum Cladding T is maximum (value °C)	[s]	145 (469°C)	182 (461°C)	139 (452°C)	156 (469°C)	140 (454°C)	
10	Coolant T @ FRSB outlet is maximum	[s]	326 (464.5°C)	200 (457.6°C)	167 (450°C)	188 (463.4°C)	145 (450.7°C)	
11	End of transient	[s]	900 (1800)	1789	1800	1800	900	

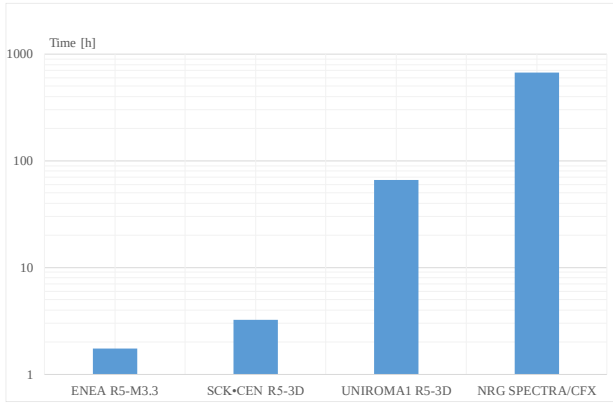

Figure 18 – CIRCE-HERO SE-Test3 benchmark: computing time.

Power balance. The power transferred from the FRSB heat structure to the fluid has been imposed by the participants, as summarized in *Table 1*. The comparison of the HERO performances as estimated by the participants is shown in *Figure 19*. The heat transferred from the primary to secondary side, during the gas enhanced circulation reduction, decreases faster in ENEA simulation. UNIROMA1 calculates the larger energy removal from the primary side from steady state up to about 120 s. After the first phase, power removed is comparable (i.e. in the range of ±20%).

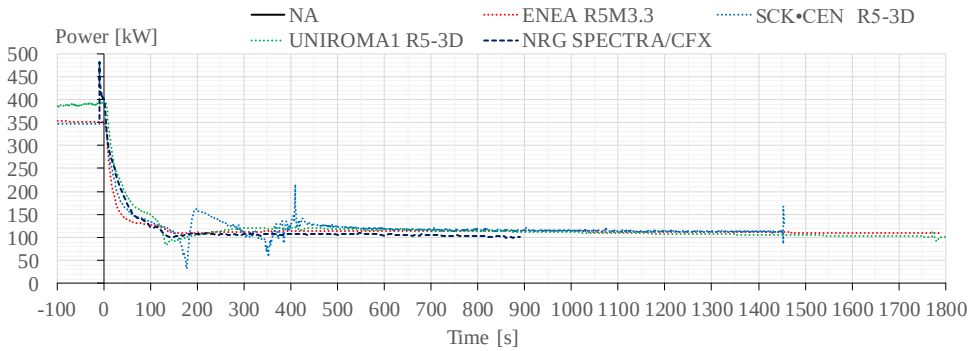

Figure 19 – CIRCE-HERO SE-Test3 benchmark: primary to secondary power exchanged.

Mass flow rates. The mass flow rate of the LBE and feedwater system are reported in *Figure 20* and *Figure 21*, respectively. In particular, the latter represents the time trends of the feedwater mass flow rate in each of the seven DWBTs for both experimental and numerical values. According to *Figure 7*, the experimental data reported are the measurements of the available TFMs (i.e. TFM-T0, TFM-T3, TFM-T4, TFM-T5), converted from cc/min (measure unit of the direct measurement) in kg/s in order to be consistent with the numerical values. The total secondary mass flow rate is imposed, as boundary conditions in the codes simulations. Indeed, the nodalizations of UNIROMA1 and SCKCEN model the DWBT one by one. The mass flow rate through the seven DWBTs does not assume uniform value in UNIROMA1 calculation. Indeed, the experimental acquisitions of the temperature at the DWBTs outlets highlighted not uniform conditions (Lorusso et al., 2019a). For this reason, in UNIROMA1 model, the pressure drops at the DWBTs inlets have been calibrated in order to obtain a prediction of the outlet conditions in each tube, under full power operation. ENEA and NRG models the 7 tubes with a single equivalent component, therefore the total calculated feedwater mass flow rate is divided by the number of tubes.

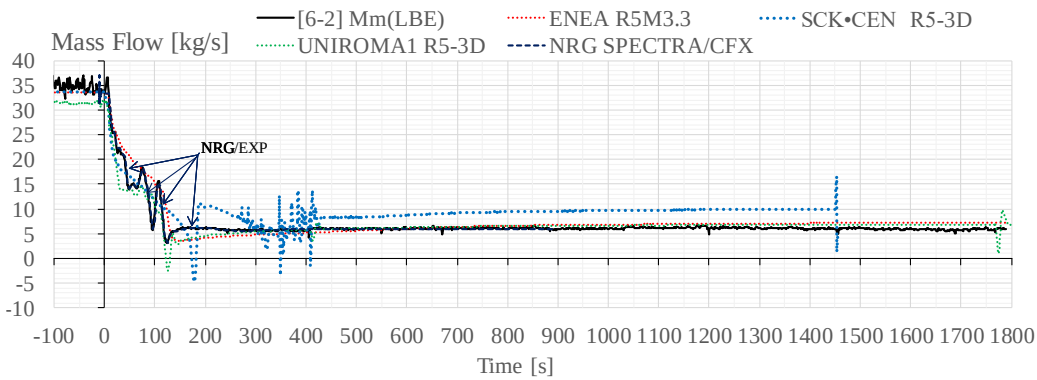

Figure 20 – CIRCE-HERO SE-Test3 benchmark: primary system LBE mass flow rate.

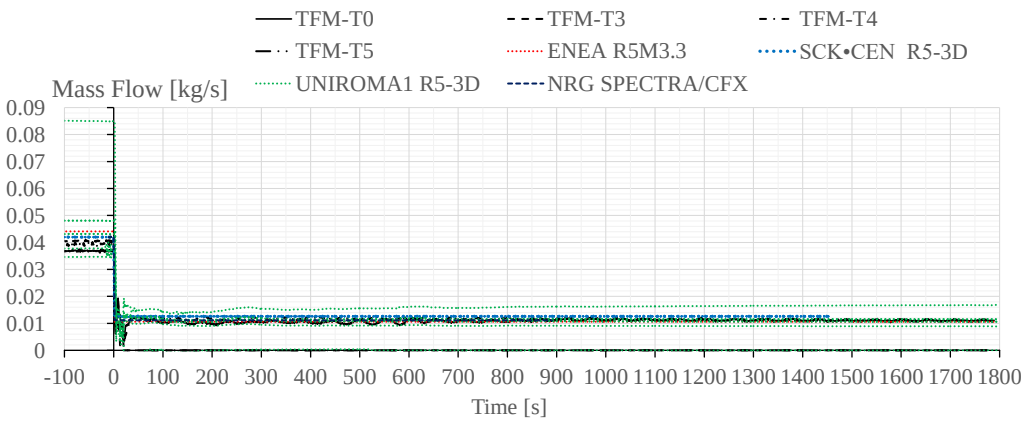

Figure 21 – CIRCE-HERO SE-Test3 benchmark: feedwater mass flow rate at each DWBT inlet.

The comparisons between the experimental data and the calculated results of the primary mass flow rate bring to the following considerations:

- ENEA predicts the primary mass flow rate with a reasonable accuracy. The simplified modelling of the gas injection system does not allow the detailed modelling of the oscillations observed in the experimental data during the gas injection reduction. Moreover, it is observed a delay of about 10 s, connected with the switching off of the gas injection line. The mass flow rate is under-predicted in the time spam 125-250 s. Then, experimental data and calculated time trend are in good agreement.
- UNROMA1 predicts the primary mass flow rate with a reasonable accuracy. During the first 110 s of the transient, the mass flow rate predicted by the code well reproduces the experimental data. When gas injection stops, the mass flow rate decreases fast and a temporary reverse flow is predicted. Then, experimental data and calculated time trend are in good agreement. Further analysis on this topic were performed during the post-test phase and are summarized in Narcisi et al. (2019c). Post-test analysis showed the relationship between the reverse flow and the distribution of the overall pressure drops. Thermal-hydraulic model adopted in the benchmark exercise provides a good estimation of the overall pressure losses, proved by the agreement with the experimental acquisition after the transition phase (see Figure 20). However, post-test activity highlighted an overestimation of the pressure drops across the SG and an under prediction of the pressure losses through the cold leg. When primary flow rate assumes low values, LBE mass flow across the SG is temporary stopped, free level within the separator increases and reverse flow conditions in the hot leg are predicted. In the analysis presented in Narcisi et al. (2019c), the distribution of the pressure drops through the primary flow path was improved and the reverse flow was suppressed. Furthermore, UNIROMA1 model predicts quite well the mass flow rate oscillations during the transient. This could be due to the more detailed axial discretization of the model, as well as the adoption of the sub-channel model of the FPS and the 3D pool model.
- SCKCEN calculation evidences an important flow inversion, larger than in UNIROMA1 simulation, when the Ar injection is stopped. The mass flow rate in natural circulation is overestimated by SCKCEN, but this could be expected since a unique pipe is used to represent the pool and one single volume for the lower plenum. Indeed, there is an underestimation of the energy dissipated in the 1D pool model and lower plenum, compared to the 3D pool models used by UNIROMA1 and parallel pipes with cross flow considered by ENEA. This effect has already been observed, in past validation activities based on CIRCE and NACIE facilities data (Bandini et al, 2011). In the other hand, overestimated natural circulation justifies the faster coolant temperature cool-down rate discussed above.
- NRG has imposed the time trend, since the calculated values overlap the experimental data.

Primary system coolant temperatures – FRSB. *Figure 22* depicts the time trends of the LBE coolant temperature in different elevations along the FRSB. Concerning UNIROMA1, which adopts a subchannel modelling approach, three temperatures are reported per each figure, calculated in the instrumented subchannels. In the FRSB zone, good predictions of the code simulations are achieved in the first part of the transient, up to 120 s. NRG highlights a slower temperature decrease at the beginning of the transient that might be connected with the different timing of the imposed boundary conditions, as reported in *Table 9*. From about 120 s up to about 145 s the coolant temperature rises and some deviations are observed. UNIROMA1 and SCKCEN overestimate the peak temperature, whereas ENEA and NRG show good agreement. Some differences are also observed regarding the time of peak whereas the time of their minimum is well estimated. These differences are connected with the differences in the behavior of the mass flow rate (*Figure 20*), which is driven by the correct simulation of the gas injection line. This would require the real layout and behavior of the gas injection line of the facility (i.e. length >15 m after the mass flow measurement, having the last part of the gas pipe descending inside the pool). Indeed, the temperature spikes connected with the sharp variation/oscillation of the mass flow rate are visible both in the experimental data and in the code simulations (SCKCEN and UNIROMA1). After 150 s, the temperature trends decrease smoothly. In this phase, the codes predict a temperature decrease faster than the experimental evidence, being the fluid conduction and the thermal diffusion becoming more relevant. These effects are not modelled in SYS-TH codes. This is highlighted in FRSB outlet section, where the experimental data are more scattered than in the time span from 30-150 s and the differences from the experimental data time trends and the code results are larger.

Figure 23 provides the comparisons of the calculated and experimental time trends of the cladding temperature at different elevations. The time trends of parameters are analogous to the ones already discussed for the coolant temperature trends.

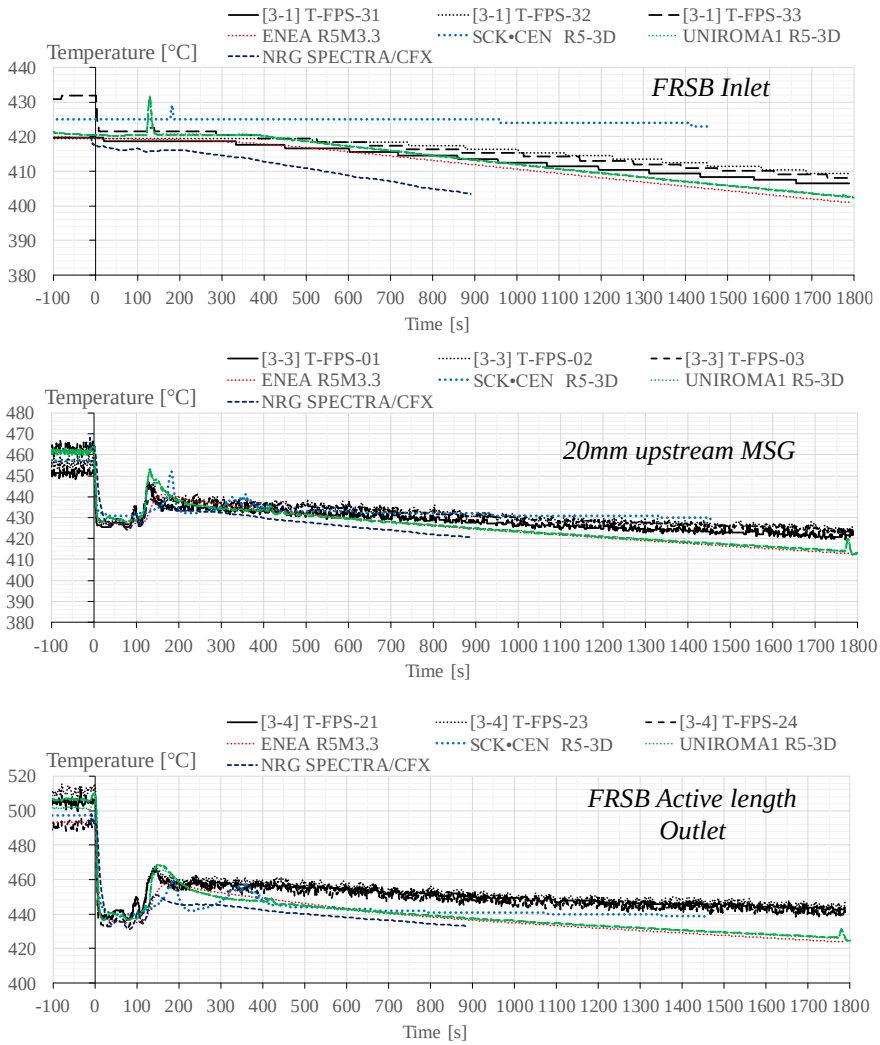

Figure 22 – CIRCE-HERO SE-Test3 benchmark: FRSB LBE temperatures at different elevations.

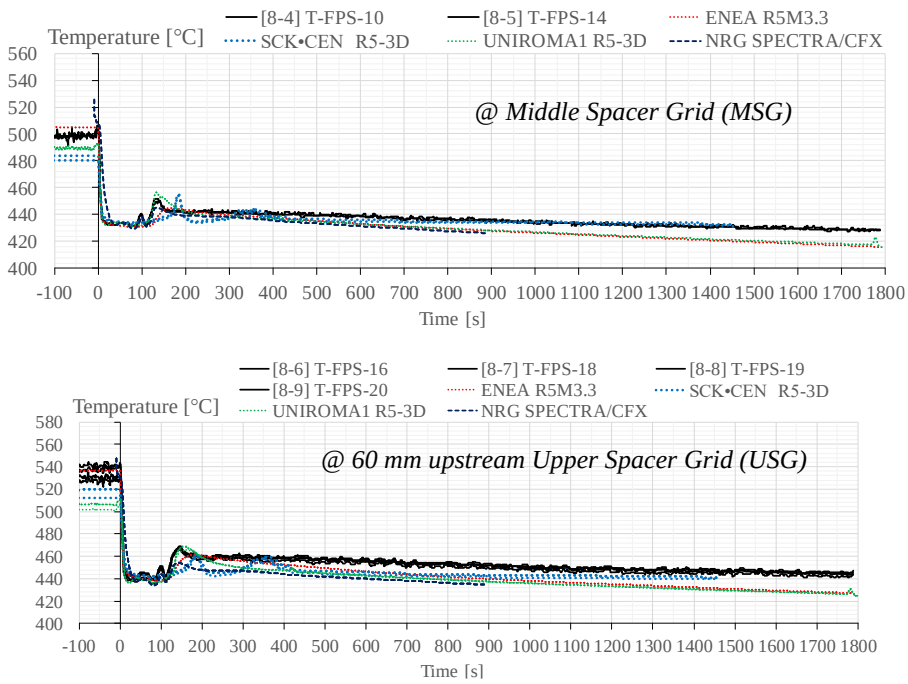

Figure 23 – CIRCE-HERO SE-Test3 benchmark: cladding temperatures - T Pin 10 and 14 @ MSG and T Pin 16, 18, 19 and 20 @ 60mm upstream USG.

Primary system coolant temperatures – HERO. *Figure 24* shows the time trends of the LBE coolant temperature at the HERO inlet and outlet sections. *Figure 25* reports the time trends at different elevations of the descending part, in particular (assuming level 0.0 mm the SG outlet), at level +4200 mm, at level +3000 mm and at level +1500 mm. Looking at the coolant temperatures recorded by three thermocouples in the separator zone (HERO inlet section) and considering their positions (Pesetti et al. (2018a), it can be noticed that the temperature measured at the inlet by TC-SG-01 suffers from instability in forced circulation respect to the other two TCs, most likely due to its position in the separator. In fact, this TC is directly exposed to the rising LBE, mixed to the argon injected at the bottom of the riser and this turbulence could affect the measure acquired. At these positions, the codes overestimate the average temperature in the separator during the steady state and in the first part of the transient (up to about 200 s). Afterwards, the codes predict a cool-down rate larger than the experimental evidence, with the exception of the ENEA results. This better agreement of ENEA could be explained considering that ENEA used a convective heat transfer correlation which is more suitable for bundle geometries respect to the ones implemented in the other codes.

Moreover, it must be noted that while ENEA has used a heat transfer model suitable for HLM and large pitch, UNIROMA1 and SCKCEN have employed standard correlations adjusting the fouling factor to match the steady state conditions. Besides, this approach has been used also in other benchmarks (e.g. IAEA, 2014c), the accuracy of the results is penalized when the mass flow rate changes towards lower values.

Finally, LBE coolant might have formed compounds in the cold parts of the system, such as the SG. These are attached to the external face of the tubes causing an additional thermal resistance. This effect discussed in Shin et al., 2019 can have further contributed to the differences between the experimental results and code simulations. Nevertheless, this is only a hypothesis which can be verified dismantling the test section, with the visual examination of the HERO SG.

Figure 26 reports the wall temperature trends, LBE side, at different elevations, i.e. +1500 mm, +3000 mm and +4200 mm from the bottom of HERO test section.

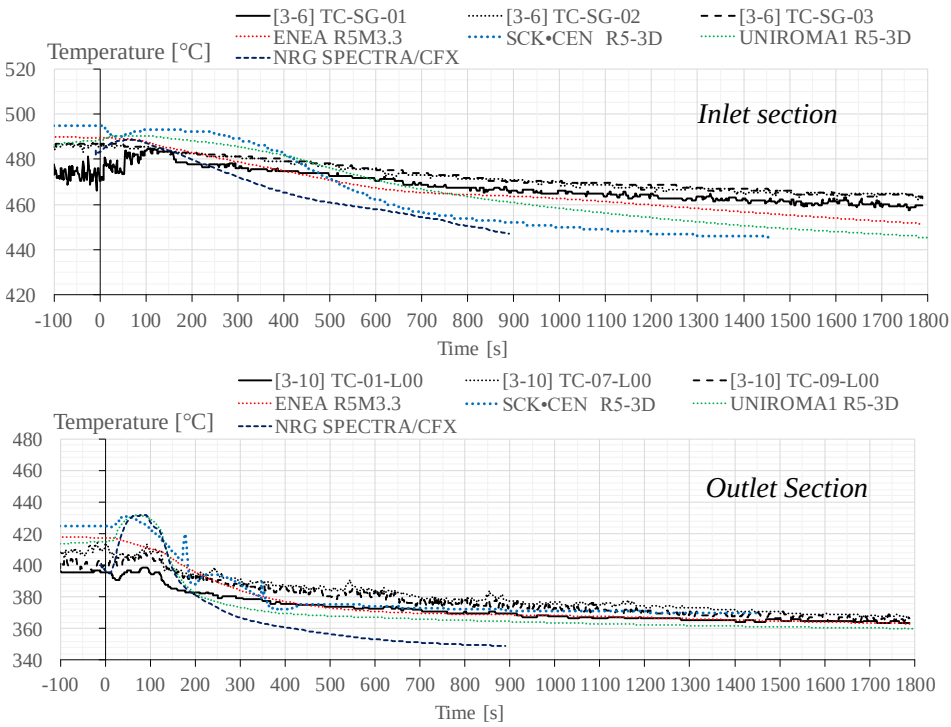

Figure 24 – CIRCE-HERO SE-Test3 benchmark: LBE temperatures at the HERO inlet and outlet sections

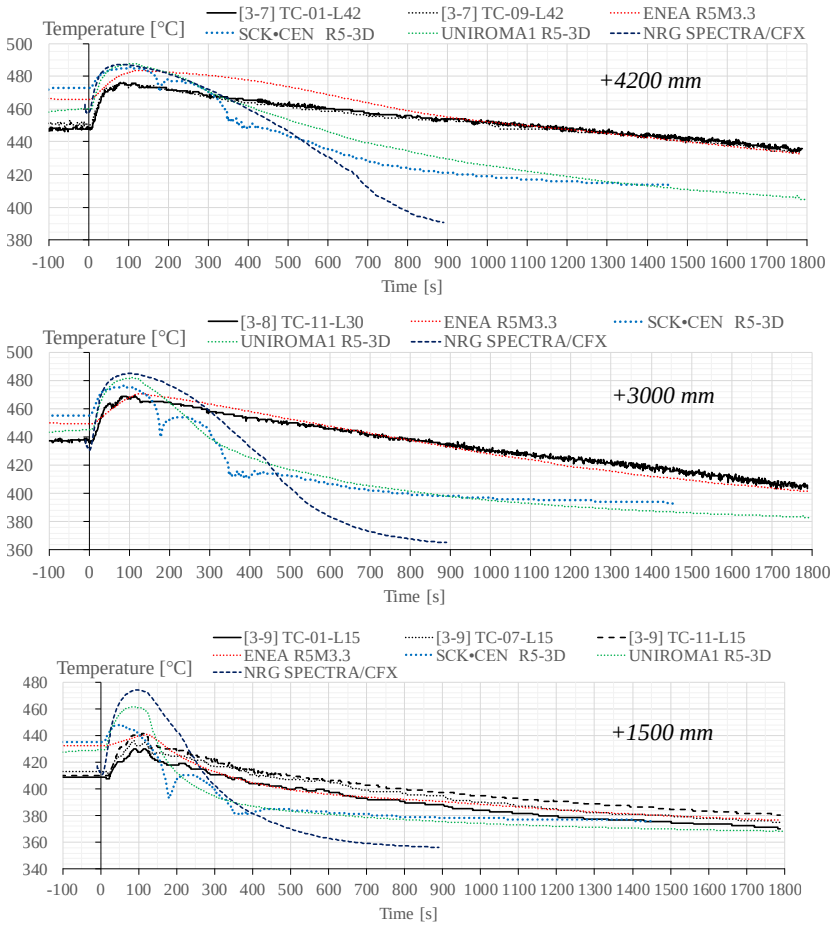

Figure 25 – CIRCE-HERO SE-Test3 benchmark: LBE temperatures along the HERO LBE side, at different elevations

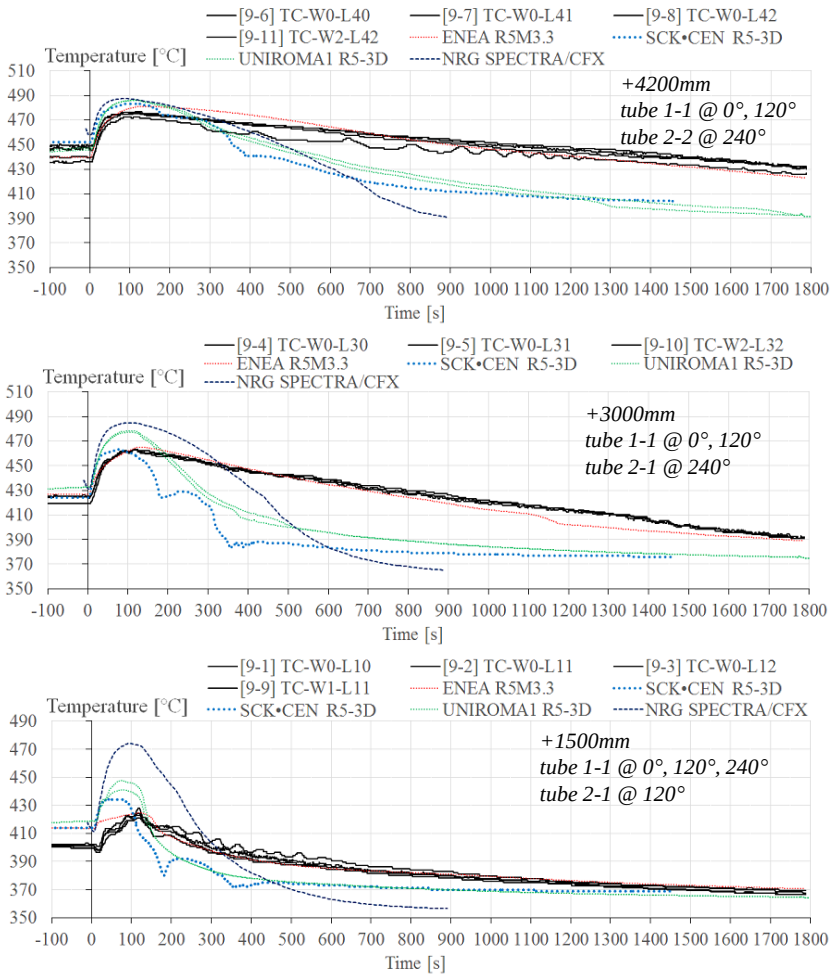

Figure 26 – CIRCE-HERO SE-Test3 benchmark: HERO LBE side wall temperatures at different elevations.

Experimental data and code results show a qualitative trend, which is analogous to the corresponding time trends of the fluid at the same elevations. Nevertheless, the code simulations are more accurate in predicting the wall temperature measurements than the LBE temperatures show a the accuracy is better than LBE coolant temperature simulations, This is visible in steady state, while it is less evident during transient. It is observed that the temperature difference between the coolant and the wall is remarkable lower in the experimental data (few degrees) than in the code simulations (about 20-30°C) during the steady state. A possible explanation of these discrepancies could be found in the heat transfer correlations used by the codes. Moreover, also the numerical modeling of the LBE channel could lead to the simulation of a thermo-dynamic behavior which could be the consequence of averaged values and does not reproduce the sub-channels effects. A further contribution to these differences could be found in the uncertainties related to the operative parameters during the test (e.g. water distribution among the 7 BTs, TCs uncertainties) (Martelli et al., 2020). When the LBE and feedwater coolant mass flow rates decrease, during the transition from forced to natural circulation, before, and the natural circulation, after, this temperature differences are reduced and result comparable with the experimental evidence.

Primary system coolant temperatures – pool. The LBE temperature profiles in the pool zone are reported in *Figure 27*. Among the TCs supporting rods described in Pesetti et al. (2018a), line A has been reported in this paper, since it is the rod with the higher number of TCs installed. The temperature vs height trend is reported at three different times, 0 s, 800 s and 1400 s. The analysis of experimental data (Lorusso et al., 2019a) shows that the pool temperature results approximately uniform in each horizontal section. This is observed also in the code simulations.

For what concern the thermal stratification in the pool, it is observed the good simulation results of NRG, modelling the pool with the CFD code. Nevertheless, beside less accurate, the SYS-TH codes simulations provide a satisfactory reproduction of the phenomenon. Indeed, comparing the trends at the different times during steady state and the transient phases, it is observed that, whereas the temperature transition zone becomes less steep at increased timing, the SYS-TH codes show the same thermal gradient. It should be noted that the 3D nodalization of UNIROMA1 provides better predictions that the 1D modelling approaches of ENEA and SCKCEN.

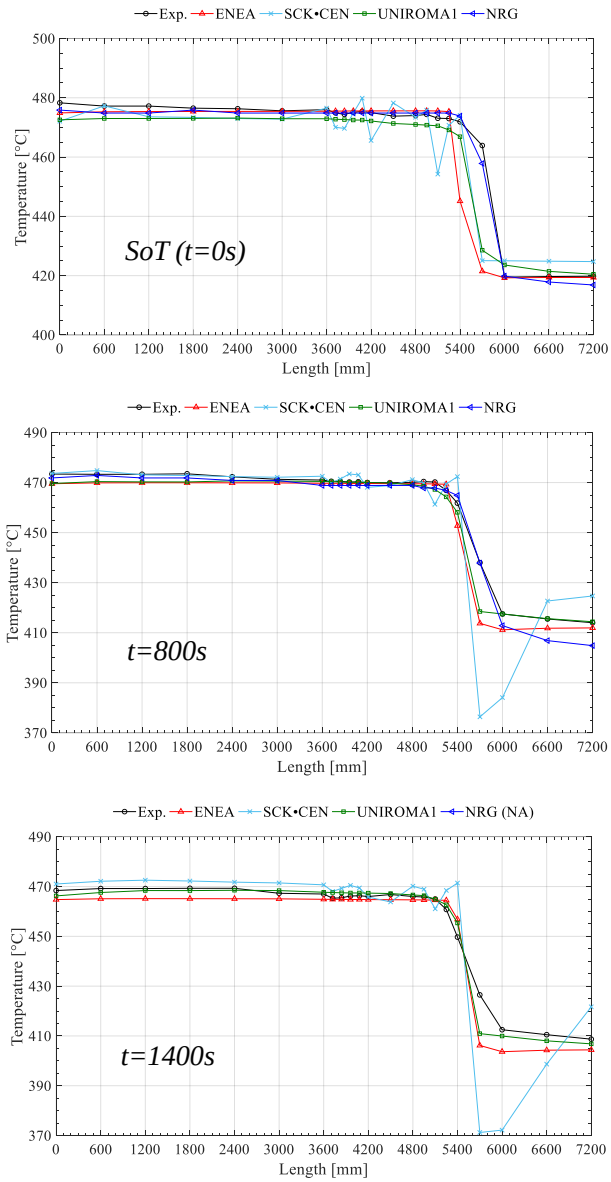

Figure 27 – CIRCE-HERO SE-Test3 benchmark: pool LBE temperature profile along vertical direction at different times, line A [0.0, -7.2m], 22 TC.

Secondary system coolant temperatures. *Figure 28* shows the temperature of the steam at the DWBT outlet and in the steam line. The codes simulations evidence a general over-prediction of the steam temperature in the first part of the transient, and a faster temperature decrease after the temperature has reached the peak. Indeed, these time trends reflect the temperature behavior of the primary side, already discussed above. Concerning UNIROMA1 simulations, the imposition of different K-loss coefficient at the DWBTs inlet leads to a spread of the distribution of the secondary flow rate (see section 3.2). Although it allows a good prediction of the full power condition, it determines a larger temperature spread than the experimental acquisitions after the transition event (green lines in *Figure 28*).

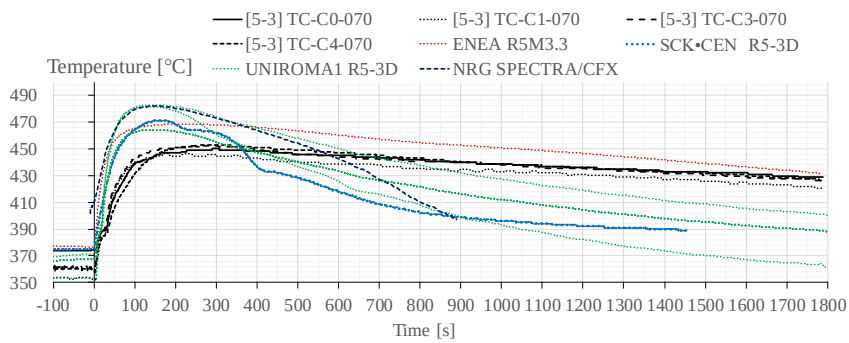

Figure 28 – CIRCE-HERO SE-Test3 benchmark: DWBT SG outlet, water temperatures.

5 CONCLUSIONS

The objective of the present paper is to collect, analyse and illustrate the post-test calculations, describing the performances of the codes simulations in large heavy liquid metal pool. The objective is fulfilled through comprehensive comparisons based on the following steps:

- comparison of the features of the analytical models applied;
- verification of the code performance at steady state;
- assessment of the code performance in transient based on the comparison and the qualitative evaluation of reference results.

The main achievements of the benchmark activity and specific outcomes from the analyses are summarized as follows.

- The test SE-Test3 constitutes a contribution for improving the validation matrices of advanced computer codes.
- The assessment database of computer codes, in relation to the HLM technology, is enlarged including the PLOFA transient in CIRCE-HERO facility.
- The capability of the codes to deal with the relevant phenomena involved in the transient is assessed.
- SYS-TH codes appear adequate in predicting the trend of the main parameters with quite satisfactory accuracy. In particular, these are the coolant and cladding temperatures, heat transfer primary to secondary side, natural circulation. Mismatches between the experimental data and code results are identified and discussed. In particular, at the steady state, the code simulations show overestimations of the LBE coolant temperatures in the intermediate positions of the SG, whereas the wall temperatures are reasonably well predicted, excepting for UNIROMA1, which had larger error.
- SYS-TH/CFD simulation provided a satisfactory representation of the thermal stratification in the pool, which resulted to be more accurate than the SYS-TH standalone simulations.
- The experimental uncertainty of the gas injection system and the simplified modelling assumptions constitutes the main reasons of the differences in the mass flow rate simulation in the first part of the transient, up to the time at which the gas injection stops.
- The use of only 1D representation of all volumes provides acceptable results for temperature and flow during steady state up to the end of argon injection, besides improvements are possible using more complex nodalization approaches (i.e. parallel pipes and cross junctions) or the multidimensional features of RELAP5-3D code. In these last cases, concerns are raised regarding the determination/validation of the cross flow pressure losses.
- The heat losses affect pool stratification. Simulation of this phenomenon is not straightforward and challenges the modelling approaches to overcome the predictive limitation of system codes. Results demonstrate the better accuracy of CFX simulation and the improvements in system codes prediction, increasing the number of nodes in the nodalization.

In general, it can be noted that the better agreement with the experimental data has been achieved by the system codes respect to the SYS-TH/CFD coupled codes. This result is due to the better knowledge concerning the use of system codes, which have been already involved in a Verification and Validation (V&V) process since many years. Contrariwise, the SYS-TH/CFD coupled codes are at a less mature stage and they need further development and improvements.

Finally, this benchmark exercise shown as further improvements on numerical models and coupling approaches are needed. This in turn is requiring to design and to run experiments fully devoted to V&V, for which the monitoring of experiments is strengthened. For this last aspect, the lesson learned from the operation of CIRCE-HERO has suggested to install:

- additional thermocouples on the external surface of the main vessel to characterize with better accuracy the heat losses from the main pool to the environment;
- additional differential pressure measurement points along the test section for a better hydraulic characterization of the components;
- an oxygen control system on CIRCE in order to control the oxide formation inside the primary coolant;
- additional thermocouples to be installed in LBE and water sides of HERO SGBT for a better monitoring of the coolants temperature profiles, as well as in the powder gap to achieve feedback on the powder heat exchange capabilities.

ACKNOWLEDGMENT

This work was performed in the framework of H2020 SESAME project. This project has funded by the European Commission under grant agreement No 654935.

ABBREVIATIONS

ALFRED Advanced Lead cooled Fast Reactor European Demonstrator

BAF	Bottom of Active Fuel
CIRCE	CIRColazione Eutettico (Eutectic CIRCulation)
CRP	Coordinated Research Project
CV	Control Volume
DHR	Decay Heat Removal
DWBT	Double Wall Bayonet Tube
FRSB	Fuel Rod Simulator Bundle
HERO	Heavy liquid mEtal – pRessurized water cOoled tube
HLM	Heavy Liquid Metal
HTC	Heat Transfer Coefficient
IAEA	International Atomic Energy Agency
ICE	Integral Circulation Experiment
INL	Idaho National Laboratory
ISP	International Standard Problem
LBE	Lead-Bismuth Eutectic
LWR	Light Water Reactor
MSG	Middle Spacer Grid
NC	Natural Circulation
NEA/CSNI	Nuclear Energy Agency - Committee on the Safety of Nuclear Installations
PLOFA	Protected Loss of Flow Accident
RC	Research Centre
SESAME	Simulations and Experiments for the Safety Assessment of MEtal cooled reactors
SG	Steam Generator
SGBT	Steam Generator Bayonet Tube
SPECTRA	Sophisticated Plant Evaluation Code for Thermal-Hydraulic Response Assessment
SYS-TH	SYStem Thermal-Hydraulic
SoT	Start of Transient
TAF	Top of Active Fuel
TC	Thermocouple
TFM	Turbine Flow Meter
TS	Test Section
USG	Upper Spacer Grid
V&V	Verification and Validation

REFERENCES

Annunziato, A., Glaeser, H., Lillington, J., Marsili, P., Renault, C., Sjöberg, A., 1996. CSNI Integral Test Facility Validation Matrix for the Assessment of Thermal-Hydraulic Codes for LWR LOCA and Transients, NEA/CSNI/R(96)17.

ASHRAE Handbook – Fundamentals, 2009.

Balestra, P., Giannetti, F., Caruso, G., Alfonsi, A., 2016. New RELAP5-3D lead and LBE thermophysical properties implementation for safety analysis of Gen IV reactors. Sci. Technol. Nucl. Install. 2016. https://doi.org/10.1155/2016/1687946.

Bandini, G., Meloni, P., Polidori, M., Gaggini, P., Tarantino, M., Ciampichetti, A, 2011. Analysis of integral circulation and decay heat removal experiments in the LBE CIRCE facility with RELAP5 code. The 14th International Topical Meeting on Nuclear reactor Thermal hydraulics, NURETH14, Toronto, Ontario, Canada, Sep 25-30, 2011.

Bricteux, L., Duponcheel, M., Winckelmans, G., Tiselj, I., and Bartosiewicz, Y., 2012. Direct and large eddy simulation of turbulent heat transfer at very low Prandtl number: Application to lead-bismuth flows. Nuclear Engineering and Design, 246. 91-97.

Davis, C.B., Shieh, A. S., 2000. Overview of the Use of ATHENA forThermal-Hydraulic Analysis of Systems with lead bismuth coolant, Proceeding of the 8th International Conference on Nuclear Engineering. April 2, 2000.

Del Nevo, A., Lorusso, P., Tarantino, M., Zwijsen, K., Breijder, P.A., Hamidouche, T., Castelliti, D., Rozzia, D., Narcisi, V., Giannetti, F., Caruso, G., Benchmark Report: Post-Test Simulations of Total Loss of Flow Test, CI-I-R-389, ENEA report, May, 30, 2019.

Forgione, N., Castelliti, D., Gerschenfeld, A., Polidori, M., Del Nevo, A., Hu, R., 4 - System thermal hydraulics for liquid metals, in F. Roelofs (2019), pp. 157-184, 1st Edition, Woodhead Publishing, 2018. DOI: 10.1016/B978-0-08-101980-1.00004-1.

Frignani, M, Alemberti, A., Villabruna, G, Adinolfi, R., Tarantino, M., Grasso, G., Pizzuto, A., Turcu, I., Valeca, S., 2017. ALFRED: A Strategic Vision for LFR Deployment. ANS Winter Meeting 2017, Washington, D.C., October 29-November 2, 2017.

Giannetti F., Vitale Di Maio D., Naviglio A., Caruso G., 2016. Thermal-hydraulic analysis of an innovative decay heat removal system for lead-cooled fast reactors. Nucl. Eng. Des., vol. 305, pp. 168-178. http://dx.doi.org/10.1016/j.nucengdes.2016.05.005.

Hamidouche, T., 2013. Assessment of RELAP5 models and correlations for LBE. SCK•CEN-I-371.

IAEA, 2002. Accident Analysis for Nuclear Power Plants, Safety Reports Series No. 23, Vienna 2002.

IAEA, 2014a. Benchmark Analyses of Sodium Natural Convection in the Upper Plenum of the MONJU Reactor Vessel, IAEA-TECDOC-1754, Vienna, 2014.

IAEA, 2014b. Control Rod Withdrawal and Sodium Natural Circulation Tests Performed during the PHENIX End-of-Life Experiments, IAEA-TECDOC-1742, Vienna, 2014.

IAEA, 2014c. Evaluation of Advanced Thermohydraulic System Codes for Design and Safety Analysis of Integral Type Reactors, IAEA-TECDOC-1733, Vienna, 2014, pp. 1 – 394, ISBN: 978-92-0-100414-0.

IAEA, 2017. Benchmark Analysis of EBR-II Shutdown Heat Removal Tests, IAEA-TECDOC-1819, Vienna, 2017.

Idelchik, I.E., 1986. Handbook of Hydraulic Resistance. Second ed. Hemisphere Publishing Corporation.

ISL Inc, RELAP5/Mod3.3 code manual volume I: code structure, system models, and solution methods, Nuclear Safety Analysis Division, July 2003.

Kazimi, M. S., Carelli, D., 1976. Clinch River Breeder Reactor Plant heat transfer correlation for analysis of CRBRP assemblies. CRBRP-ARD-0034.

Lorusso, P., Bassini, S., Del Nevo, A., Di Piazza, I., Giannetti, F., Tarantino, M., Utili, M., 2018a. GEN-IV LFR development: status & perspectives. Prog. Nucl. Energy 105 (2018), 318–331. https://doi.org/10.1016/j.pnucene.2018.02.005.

Lorusso, P., Pesetti, A., Tarantino, M., 2018b. ALFRED Steam Generator Assessment: design and pre-test analysis of HERO experiment, Proceedings of the 2018 26th International Conference on Nuclear Engineering, July 22-26, 2018, London, England, ICONE26-81824, doi: 10.1115/ICONE26-81824.

Lorusso P., Pesetti A., Tarantino M., Narcisi V., Giannetti F., Forgione N., Del Nevo A., 2019a. Experimental Analysis Of Stationary And Transient Scenarios Of ALFRED Steam Generator Bayonet Tube In CIRCE-HERO Facility, Nuclear Engineering and Design 352 (2019) 110169, https://doi.org/10.1016/j.nucengdes.2019.110169.

Lorusso P., Pesetti A., Barone G., Castelliti D., Caruso G., Forgione N., Giannetti F., Martelli D., Rozzia D., Van Tichelen K., Tarantino M., 2019b, MYRRHA primary heat exchanger experimental simulations on CIRCE-HERO, Nuclear Engineering and Design 353C (2019) 110270, https://doi.org/10.1016/j.nucengdes.2019.110270.

Lorusso P., Pesetti A., Tarantino M., Narcisi V., 2019c. Protected Loss Of Flow Accident Simulation In Circe-Hero Facility: Experimental Test And System Code Assessment, Proceedings of the 2019 27th International Conference on Nuclear Engineering, May 19-24, 2019, Tsukuba, Ibaraki, Japan, ICONE27-2269.

Martelli, E., Giannetti, F., Ciurluini, C., Caruso, G., Del Nevo, A., 2019. Thermal-hydraulic modeling and analyses of the water-cooled EU DEMO using RELAP5 system code, Fusion Eng. Des., (2019), DOI: 10.1016/j.fusengdes.2019.02.021.

Martelli, E., Del Nevo, A., Lorusso, P., Giannetti, F., Tarantino, M., 2020. Investigation of heat transfer in a steam generator bayonet tube for the development of PbLi technology for EU DEMO fusion reactor, Fusion Engineering and Design 159 (2020) 111772, https://doi.org/10.1016/j.fusengdes.2020.111772.

Mikityuk, K., 2009. Heat transfer to liquid metals: Review of data and correlations for tube bundles, Nuclear Engineering and Design 239(4):680-687, DOI: 10.1016/j.nucengdes.2008.12.014.

Narcisi, V., Giannetti, F., Tarantino, M., Martelli, D., Caruso, G., 2017. Pool temperature stratification analysis in CIRCE-ICE facility with RELAP5-3D© model and comparison with experimental tests. Journal of Physics: Conference Series, 923 (1), art. no. 012006, DOI: 10.1088/1742-6596/923/1/012006.

Narcisi V., Giannetti F., Del Nevo A., Tarantino M., Caruso G., 2018. Pre-test analysis of accidental transients for ALFRED SGBT mock-up characterization. Nucl. Eng. Des., vol. 333, pp. 181-195. https://doi.org/10.1016/j.nucengdes.2018.04.015.

Narcisi V., Giannetti, F., Del Nevo, A., Alcaro, F., Wang, X., Kraus, A., Brunett, A., Thomas, J., Girault, N., Grosjean, B., Caruso, G., Gerschenfeld, A., 2019a. System thermal-hydraulic modelling of the phénix dissymmetric test benchmark. Nucl. Eng. Des., vol. 353, 110272. https://doi.org/10.1016/j.nucengdes.2019.110272

Narcisi V., Giannetti F., Caruso G., 2019b. Investigation on RELAP5-3D© capability to predict thermal stratification in liquid metal pool-type system and comparison with experimental data. Nucl. Eng. Des., vol. 352, 110152, https://doi.org/10.1016/j.nucengdes.2019.110152.

Narcisi V., Giannetti F., Caruso G., 2019c. Post-test simulation of a PLOFA transient test in the CIRCE-HERO facility. Nucl. Eng. Des., vol. 355, 110321, https://doi.org/10.1016/j.nucengdes.2019.110321.

NEA-Handbook, 2007. Handbook on Lead-bismuth Eutectic Alloy and Lead Properties, Materials Compatibility, Thermal-hydraulics and Technologies.

OECD/NEA, 2000. CSNI International Standard Problems (ISP) – Brief Descriptions (1975-1999), NEA/CSNI/R(2000)5.

OECD/NEA Nuclear Science Committee, 2015. Handbook on Lead-bismuth Eutectic Alloy and Lead Properties, Materials Compatibility, Thermal- hydraulics and Technologies. https://www.oecd-nea.org/science/pubs/2015/7268-leadbismuth-2015.pdf.

Oriolo, F., De Varti, A., Fruttuoso, G., Leonardi, M., Bocci, S., Forasassi, G., 2000. Modifiche del Codice RELAP5 versione MOD3.2 per la Simulazione di Sistemi Refrigerati con leghe di Pb o Pb-Bi, RL 031/00, Università di Pisa, Novembre 2000.

Pesetti, A., Tarantino, M., Gaggini, P., Polazzi, G., Forgione, N., 2017. Commissioning of CIRCE Facility for SGTR Experimental Investigation for HLMRS and Pre-Test Analysis by SIMMER-IV Code, International Conference on Nuclear Engineering, paper ICONE25-67419, Shanghai, China, DOI: 10.1115/ICONE2567419.

Pesetti, A., Forgione, N., Narcisi, V., Lorusso, P., Giannetti, F., Tarantino, M., Del Nevo, A., 2018a. ENEA CIRCE-HERO test facility: geometry and instrumentation description, ENEA report CI-I-R-343, June 2018.

Pesetti, A., Lorusso, P., Polazzi, G., Sermenghi, V., Tarantino, M., 2018b. CIRCE-HERO test facility: Heat losses charaterization tests, CI-I-R-351.

Rozzia, D., Fasano, G., Di Piazza, I., Tarantino, M., 2015a. Experimental investigation on powder conductivity for the application to double wall heat exchanger (NACIE-UP). Nucl. Eng. Des. 283, 100–113.

Rozzia, D., Fasano, G., Tarantino, M., Del Nevo, A., Forgione, N., Alemberti, A., 2015b. Experimental Investigation on Powder Conductivity for the Application to Double Wall Bayonet Tube Bundle Steam Generator, Proc. of the 24th Int. Conf. Nuc. En. for New Europe (NENE), Portoroz, Slovenia, Sept. 14-17, 2015. Paper 214, 9 pages. ISBN: 978-961-6207-38-6

Rozzia, D., Del Nevo, A., Tarantino, M., 2016. CIRCE-HERO test setup. SESAME document CI-T-R-212.

Rozzia, D., Pesetti, A., Tarantino, M., Del Nevo, A., Forgione, N., 2017. Hero test section for experimental investigation of steam generator bayonet tube of ALFRED. International Conference on Nuclear Engineering, Proceedings, ICONE, 5 doi: 10.1115/ICONE2567422.

Schikorr M., Bubelis E., Mansani L., Litfin K., 2010. Proposal for pressure drop prediction for a fuel bundle with grid spacers using Rehme pressure drop correlations. Nucl. Eng. Des., vol. 240, pp. 1830-1842, DOI: 10.1016/j.nucengdes.2010.03.039.

SESAME Project, 2015. EURATOM H2020, Grant Agreement N. 654935.

Shin, Y., Gladinez, K., Lim, J., Marino, A., Rosseel, K., Aerts, A., Van Tichelen, K., 2019. Fouling effect of lead oxide crystallization on heat transfer in LBE, 18th International Topical Meeting on Nuclear Reactor Thermal Hydraulics, NURETH 2019, Pages 1346-1359, Portland, United States.

Stempniewicz, M.M., 2017. SPECTRA Sophisticated Plant Evaluation Code for Thermal-Hydraulic Response Assessment, Version 3.61, November 2017, NRG report K6202/MSt-1771112, Arnhem, November 24, 2017. SPECTRA code.

Tarantino, M., Agostini, P., Benamati, G., Coccoluto, G., Gaggini, P., Labanti, V., Venturi, G., Class, A., Liftin, K., Forgione, N., Moreau, V., 2011. Integral Circulation Experiment: Thermal-hydraulic simulator of a heavy liquid metal reactor. Journal of Nuclear Materials, 415 (3), pp. 433-448. DOI: 10.1016/j.jnucmat.2011.04.033.

Tarantino, M., Forgione, N., Del Nevo, A., Bandini, G., 2012. Post Test Analysis of ICE Tests, Proc. of 20th Int. Conf. on Nuc. Eng. (ICONE20), Anaheim, CA, USA, July 30–August 3, 2012, Paper No. ICONE20-54952, Vol. 2, pp. 703-712, 10 pages.

Tarantino, M., Martelli, D., Barone, G., Di Piazza, I., Forgione, N., 2015. Mixed convection and stratification phenomena in a heavy liquid metal pool. Nucl. Eng. Des. 286, 261–277. https://doi.org/10.1016/j.nucengdes.2015.02.012.

The RELAP5-3D© Code Development Team, 2015. RELAP5-3D© Code Manual Volume I: Code Structure, System Models and Solution Methods, INL/MIS-15-36723, Revision 4.3.

Uitslag-Doolaard, H.J., Alcaro, F., Roelofs, F., Wang, X., Kraus, A., Brunett, A., Thomas, J., Geffray, C., Gerschenfeld, A., 2019. Multiscale modelling of the Phénix Dissymmetric Test Benchmark. Nucl. Eng. Des. 356, 110375. https://doi.org/10.1016/j.nucengdes.2019.110375

Umminger, K., Del Nevo, A., 2012. Integral Test Facilities and Thermal-Hydraulic System Codes in Nuclear Safety Analysis, Science and Technology of Nuclear Installations, vol. 2012, Article ID 826732. DOI: 10.1155/2012/826732.

Ushakov P.A., Zhukov A.V., Matyukhin N.M., 1977. Heat transfer to liquid metals in regular arrays of fuel elements. High Temp. vol. 15, pp. 868–873 translated from Teplofizika Vysokikh Temperatur, vol. 15 (1977), pp. 1027–1033.